IEEE Access
Multidisciplinary | Rapid Review | Open Access Journal

Received March 7, 2022, accepted March 23, 2022, date of publication March 30, 2022, date of current version April 8, 2022.

Digital Object Identifier 10.1109/ACCESS.2022.3163299

Fixed Settling Time Control for Self-Driving Car: Two-Timescales Approach

RAMEEZ KHAN[1], RAJA AMER AZIM[1], FAHAD MUMTAZ MALIK[1], NAVEED MAZHAR[1], ABID RAZA[1], AND HAMEED ULLAH[2]

[1]College of Electrical and Mechanical Engineering, National University of Sciences and Technology, Islamabad 44000, Pakistan
[2]PRISMA Laboratory, Department of Electrical Engineering and Information Technology (DIETI), University of Naples Federico II—UNINA, 80138 Naples, Italy

Corresponding author: Rameez Khan (rameez.khan@ceme.nust.edu.pk)

This work was supported by the National University of Sciences and Technology, Islamabad, Pakistan.

ABSTRACT This article involves the design of a novel path tracking control technique for the self-driving car. Fixed settling time sliding mode control (FSTSMC) with barrier Lyapunov function is implemented to deal with the non-linear lateral dynamics and to ensure stable standard double-lane-change (DLC) maneuver of self-driving cars in the presence of unknown lateral tire forces and parametric uncertainties. A two-time scale-based approach is employed to deal with the slow and fast dynamics of the car separately. The proposed control scheme efficacy is investigated using simulations based on CarSim and Simulink. The simulation results validate the path-tracking ability of the proposed controller for self-driving cars while accomplishing the stable double-lane-change maneuver at various forward speeds.

INDEX TERMS Autonomous vehicles, barrier function, CarSim, double-lane-change (DLC), fixed settling time sliding mode control (FSTSMC), lateral dynamics, self-driving car.

I. INTRODUCTION

In recent times self-driving cars have undergone rapid advancements with the evolution of intelligent transportation systems. The aptitudes of self-driving cars are demonstrated by academia and industry through Google self-driving car, DAPRA urban challenge, and Tesla self-driving cars [1], [2]. The research associated with the self-driving car is mainly focused to achieve full autonomy while ensuring passenger comfort, safety, optimal fuel consumption, and effective maneuvering on different terrains [3], [4]. It is vital that the self-driving car can maneuver efficiently which attracts the attention of academia and industry to address challenges of path tracking, obstacle avoidance, trajectory planning, and vehicle stability in the presence of unwanted disturbances and uncertain environments [5]–[9].

Among several issues associated with the motion of the self-driving car, path tracking control is one of the key concerns. Path tracking control enables the self-driving car to achieve the desired trajectory by adjusting the vehicle longitudinal and lateral motion which is achieved by calculating and adjusting the desired actuating input. Therefore, path tracking control is essential for an efficient drive of the self-driving car. In self-driving cars, both longitudinal and lateral controls are essential for path tracking [10]. The longitudinal controller deals with the problems associated with acceleration and braking on the straight path where the longitudinal dynamics become more dominant [11]. Alternatively, lateral control caters to the problems related to lane changing, safety, lane-keeping, and exhibiting the desired maneuver on the curved path where effects of the lateral dynamics become more considerable [12]–[14].

The lateral path-tracking control is of paramount importance, predominantly during critical maneuvers, while taking sharp turns and motion on the curved path. Lane change is one of the fundamental functions of lateral control [15]. It involves highly nonlinear vehicle dynamics i.e. lateral dynamics becomes dominant, hence vehicle handling stability and coupled tire forces become critical for driving safety of automated vehicles [16]. Since the lateral control of the self-driving car is responsible for both lane-changing and stability of the vehicle, therefore, a nonlinear controller is necessary to account for the system's dynamics while ensuring the stable lane-change maneuver. In this paper, a novel control approach is devised to ensure the fixed time tracking of the lateral dynamics of self-driving cars during the standard

The associate editor coordinating the review of this manuscript and approving it for publication was Chao-Yang Chen.

double-lane-change (DLC) maneuver, while keeping outputs in constraint.

There is wide-range ongoing research in the literature related to designing path tracking control schemes for the self-driving car during its lane-change maneuver. To realize this prospect different control techniques have been devised including PID [17], feedback linearization, composite nonlinear feedback [18], backstepping [19], [20], gain scheduling [21], other non-linear techniques like sliding mode control (SMC), terminal SMC [22], [23], model predictive control (MPC), adaptive neural network and fuzzy logic [24], [25]. In [22], the authors proposed a non-linear control scheme based on backstepping and SMC for the self-driving car's steering control. Another study investigated lateral dynamics control of the vehicle by employing variable structure sliding mode [26]. Another approach based on SMC and gain scheduling is presented in [27] which also used disturbance observer for the trajectory tracking problem of the vehicle. In [28] a two-layered automated lane changing controller is presented. The problem is posed as a trajectory tracking problem. In another article, the MPC algorithm is used for lane change control of lateral dynamics. The results are validated using CarSim [29]. Some other approaches to cope with the lane change problem are also discussed in several studies [30]–[32].

Most of the tracking control problems in the literature are limited to asymptotic tracking hence the required convergence time for the states is almost infinite. To overcome this problem, a finite time control scheme was presented which achieves the convergence of the state in finite time [33]. Due to dependency on the availability of the system's initial conditions the finite-time control scheme is not suited for practical applications. In order to mitigate this problem fixed time control is proposed which ensures convergence in the fixed time independent of initial conditions [34].

The fixed-time control technique is recently being used to achieve fixed-time stability which is independent of initial conditions [35], [36]. To avoid the settling time dependency on the system's initial conditions, fixed-time control technology, and the PN guidance law is proposed in [37]. In [38], singularity-free fixed-time sliding mode control is presented to achieve fixed-time tracking of robot manipulators. In another study, a fixed time backstepping-based control scheme is proposed [39]. The authors proposed path-dependent constrained operation for self-driving cars is investigated, assuming negligible friction and tire dynamics. This motivates to use fixed time control in this work.

In general, the mathematical models of self-driving cars are an extension of the 3 degrees of freedom (DOF) bicycle model. Additionally, assuming the smoothness of longitudinal dynamics as well as their separate controllability conditions the self-driving car system is reduced into a 2-DOF model that consists of yaw angle and lateral position. Ultimately, the self-driving car becomes a single-input multi-output (SIMO) system having one steering wheel angle input and two outputs, yaw angle, and lateral position. In this system, the lateral position and yaw angle appears to be slow, and fast states respectively. As a result, the lateral dynamics of self-driving cars can be reduced into slow lateral dynamics and fast lateral dynamics. A composite controller technique is typically used to control these two-timescale systems. The energy-based controllers [40], intelligent controllers [41], [42], hierarchical controllers [43]–[46], and composite controllers [47], [48] are other approaches to govern SIMO systems. The control for the self-driving car's lateral dynamics is designed using a two-timescale technique in this research.

Another crucial feature of the self-driving car is its capacity to maintain safety and stability in varying environments e.g., on road. Due to input saturation and the complex tire-terrain relation, the vehicle can maneuver in unsafe operating range. One possible solution to this challenge is to bound the system lateral states to a specific practical range i.e., by specifying the maximum yaw angle and a lateral position. Typically, a control barrier function is used to meet these requirements. [49], [50].

Output constraints are usually very important in practical applications and cannot be overlooked. K. P. Tee *et al.* [51] presented barrier Lyapunov function (BLF) as a solution to this problem. The practical systems require a priori constraints on the system states to be met due to the limitations of the systems. Nonlinear perturbed systems with state constraints include electrical circuits, mechanical devices, and mechatronic systems. In robotic manipulators, position and velocity are constrained by the mechanical design of the manipulator. The BLF is also used to ensure system error convergence to acceptable ranges while the anti-windup approach overcomes control input saturation in [52].

Robust backstepping control with BLF is proposed to counter model uncertainties and external disturbances in [53]. In another study, the authors proposed finite-time stabilization with BLF and backstepping controller for quadrotor [54]. In [55] a simple diagrammatical model is used to employ a tracking controller for a 4-wheeled electric vehicle. Moreover, the wheeled acceleration is constrained to obtain constraints on wheel slips. Using a unified synthesis framework, [56] provides a robust vibration controller architecture for active suspension systems of an electric vehicle. The authors compared the performance of the H∞ controller using the passive suspension with the proposed technique. Furthermore, finite-time trajectory tracking control of an output-constrained quadrotor with sliding mode control is presented in [49]. Similar methodology is used in applications like hypersonic flight vehicles, robot manipulators, and distributed crowd dynamics [57], [58]. Extending these approaches, BLF can be used in conjunction with SMC to guarantee fixed time stability under the output constraint.

In our recent article [59], SMC with BLF(BSMC) is implemented for lateral control of a self-driving car using a two-timescale approach. However, the non-standard control approach was used in that case. Also, the comparison of BSMC with SMC was carried out to validate the efficacy

of BSMC. Furthermore, in the previous article, convergence time was not calculated for the closed-loop system. In this article, the previous procedure is improved such that the two-timescale dynamics of a self-driving car are modified to quasi-steady-state and boundary layer models. Finally, the standard composite control is designed such that the tracking error is guaranteed to reach within small bound in fixed settling time. Moreover, in this article, the CarSim based simulations are presented to achieve the stable double change maneuver which validates the robustness of the controller.

In this article, the lateral dynamics of a self-driving car are taken into account and their two-timescale behavior is presented mathematically while performing the DLC maneuver at different forward speeds. The self-driving car is modeled using the 2-DOF perturbed bicycle model. The lateral tire forces, road curvature effects, and parametric uncertainties are modeled as disturbances with a known upper bound. As a result, a SIMO dynamical system is obtained whose outputs are yaw and lateral position while steering wheel angle acts as the system input. By nonlinear model reduction techniques, the model is reduced to slow lateral subsystem and fast lateral subsystem, following the methodology used in [60]–[62]. The slow lateral subsystem consists of lateral position dynamics while the fast lateral subsystem constitutes yaw dynamics. In this way, the complexity of the perturbed SIMO system reduces, and two separate controllers are designed for slow and fast lateral dynamics. Moreover, the approach of [49] is modified for both subsystems such that the lateral position and yaw angle remain in realistic bounds in presence of the abovementioned disturbances in fixed settling time. Finally, the proposed technique is validated using the CarSim simulator, which proves the practicality of the proposed control design procedure. It shall be noted that the vehicle dynamics in CarSim are not in two-timescale and consider all the aforementioned disturbances therefore the performance of the proposed controller is of great significance.

This article contributes to both the theory of control systems and the automotive industry. The novelty of this article is stated as follows: i) A barrier function-based sliding mode control solution is proposed for perturbed two-timescale nonlinear systems under output constraints. ii) The proposed controller guarantees the convergence of tracking error within a certain pre-set bound in fixed time, for two-timescale systems. iii) The vehicle lateral dynamics are extended to two-timescales and the proposed theory is implemented on vehicle dynamics. iv) The practicality of the results is realized using CarSim simulations for different longitudinal vehicle speeds.

The rest of the article is organized as: in section II, the necessary assumptions and lemmas for controller design are described. The self-driving car's lateral dynamics in two-time scales are modeled in section III. In section IV, FSTSMC with barrier function is presented for self-driving car's lateral dynamics control in two-time scale. In section V, the simulation results based on CarSim/Simulink are produced and discussed. The last section concludes the paper.

II. PRELIMINARIES

Consider a nonlinear system of the following form:

$$\dot{x}_1 = x_2 \tag{1}$$
$$\dot{x}_2 = f(x) + g(x)u + D(x,t) \tag{2}$$
$$y = x_1 \tag{3}$$

where the systems' states are $x_1, x_2 \in \mathbb{R}$, input $u \in \mathbb{R}$, output $y \in \mathbb{R}$ and f and g are the smooth functions and uncertainties are given by $D(x,t)$.

Definition 1 (Fixed settling time stability): Consider the system $\dot{x} = f(t,x), x(0) = x_0, f(0,0) = 0$ where $f : \mathbb{R}^{0+} \times \mathcal{D} \to \mathbb{R}^n$ is defined continuously on $\mathcal{D}$, where $\mathcal{D}$ is the open neighborhood of origin. A globally asymptotically stable origin is said to be globally fixed-settling-time stable if every solution $x(t, x_0)$ reach within a certain bound $\rho \approx 0$ in fixed time, thus $x(t, x_0) \leq \rho \forall t \geq T$ and $x_0 \in \mathbb{R}^n$. The function T is named as the fixed settling time function and is independent of the initial condition.

Remark 1: In literature, the finite/fixed time control guarantees null tracking error, which is achieved using terminal sliding mode control. By abuse of notation, in Definition 1, we assume that after fixed settling time T, the states are not exactly zero but are within a small bound. This is a practical assumption considering that often small errors (e.g., 2%) are acceptable and do exist in most of the systems. In the next section, it is elaborated that the fixed settling time control is achieved using a linear sliding manifold which simplifies the control implementation as well as avoids singularity issue.

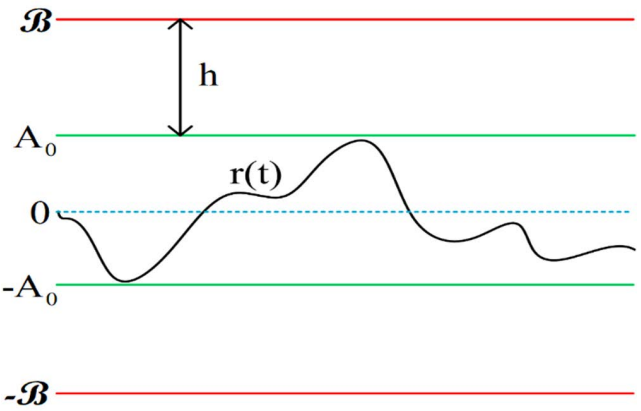

FIGURE 1. Illustration of assumption 1.

Assumption-1 ([51]): For any $\mathcal{B} > 0$, there exist positive constants $Y_0, A_0, Y_1, Y_2 \ldots Y_n$ satisfying $Y_0 \leq A_0 < \mathcal{B}$ such that the desired reference $r(t)$, as well as its successive time derivatives, satisfy $|r(t)| < Y_0, |\dot{r}(t)| < Y_1, \ldots, |r^{(n)}(t)| < Y_n$ for all $t \geq 0$.

Remark 2: The desired reference can be time-varying thus Assumption 1 makes sure that the desired reference and its successive derivatives are bounded by some constant which is less than the required constraint $\mathcal{B}$. The Figure 1 illustrates the boundaries referred in Assumption 1.

Lemma-1 ([51]): For the system (1-3) with any $\hbar_b > 0$, consider $\mathcal{E}1 := \{\xi_1 \in \mathbb{R} : -\hbar_b < \xi_1 < \hbar_b\} \subset \mathbb{R}$. Let V_1 and V_2 are positive definite and continuously differentiable functions in their respective domain as $V_1(x_1) \to \infty$ as $x_1 \to \hbar_b$ or $x_1 \to -\hbar_b$ and

$$\underline{\beta}(|x_2|) \leq V_2(x_2) \leq \overline{\beta}(|x_2|)$$

Here $\overline{\beta}$ and $\underline{\beta}$ are class $\mathcal{K}_\infty$ functions. Let V_1 and V_2 are functions that imply $V(x) = V_1(x_1) + V_2(x_2)$ and x_1 belong to the set $x_1 \in (-\hbar_b, \hbar_b)$. If

$$\dot{V} = \frac{\partial V}{\partial x}\dot{x} \leq 0 \tag{4}$$

then $x_1(t)$ remains in the open set $x_1 \in (-\hbar_b, \hbar_b)\, \forall t \geq 0$.

Lemma-2 ([63], [64]): For any positive constant a, b, the following inequalities hold:

$$(a+b)^{\wp} \leq a^{\wp} + b^{\wp}$$

where $0 < \wp \leq 1$, and

$$ln\left(\frac{a^2}{a^2 - x^2}\right) \leq \frac{x^2}{a^2 - x^2} \tag{5}$$

$\forall x$ such that $|x| < a$.

III. TWO-TIME SCALE SYSTEM MODEL

In this section, a two-time scale model for lateral dynamics of the self-driving car is presented. A four-wheeled vehicle with front-wheel steering is presented in this paper. Based on our previous paper the vehicle lateral dynamics are presented below [13], [59].

$$\ddot{y} = -\frac{2\left(C_f + C_r\right)}{m v_x}\dot{y} - \left[\frac{2\left(C_f d_f - C_r d_r\right)}{m v_x} + v_x\right]\dot{\varphi} + \frac{2C_f}{m}\delta + \frac{\tilde{F}_{fy} + \tilde{F}_{ry} + F_b}{m} \tag{6}$$

$$\ddot{\varphi} = -\frac{2\left(C_f d_f^2 + C_r d_r^2\right)}{J v_x}\dot{\varphi} - \frac{2\left(C_f d_f - C_r d_r\right)}{J v_x}\dot{y} + \frac{2C_f d_f}{J}\delta + \frac{d_f \tilde{F}_{fy} - d_r \tilde{F}_{ry}}{J} \tag{7}$$

where δ is the steering wheel angle, longitudinal speed is denoted by v_x, and φ represents yaw angle. $\tilde{F}_{fy}, \tilde{F}_{ry}$, are lateral front and rear tire forces, respectively. Moreover φ_d is desired yaw-angle while cornering stiffness coefficients for front and rear tires are denoted by C_f and C_r, respectively. F_b is road banking angle, d_f and d_r are front and rear wheels distances from CG.

The error dynamics $\dot{e_1} = \dot{y} + v_x(\varphi - \varphi_d)$ and $e_2 = \varphi - \varphi_d$ represent the lateral speed and yaw errors, respectively. The resulting model of the self-driving car in the error dynamics is given by:

$$\ddot{e}_1 = -\frac{2\left(C_f + C_r\right)}{m v_x}\dot{e_1} + \frac{2\left(C_f + C_r\right)}{m}e_2 - \frac{2\left(C_f d_f - C_r d_r\right)}{m v_x}\dot{e_2} + \left[-\frac{2\left(C_f d_f - C_r d_r\right)}{m v_x} - v_x\right]\dot{\varphi}_d + \frac{2C_f}{m}\delta + \frac{\tilde{F}_{fy} + \tilde{F}_{ry} + F_b}{m} \tag{8}$$

$$\ddot{e_2} = -\frac{2\left(C_f d_f^2 + C_r d_r^2\right)}{J v_x}\dot{e_2} - \frac{2\left(C_f d_f - C_r d_r\right)}{J v_x}\dot{e_1} + \frac{2\left(C_f d_f - C_r d_r\right)}{J}e_2 + \frac{2C_f d_f}{J}\delta + \frac{d_f \tilde{F}_{fy} - d_r \tilde{F}_{ry}}{J} - \frac{2\left(C_f d_f^2 + C_r d_r^2\right)}{J v_x}\dot{\varphi}_d - \ddot{\varphi}_d \tag{9}$$

Furthermore, we define $q_1 = e_1$; $q_2 = \dot{e_1}$; $q_3 = e_2$ and $q_4 = \dot{e_2}$ then the system takes the form:

$$\begin{cases} \dot{q}_1 = q_2 \\ \dot{q}_2 = \kappa_1 q_2 + \kappa_2 q_3 + \kappa_3 q_4 + \gamma_1 \delta + \omega_1 \end{cases} \tag{10}$$

$$\begin{cases} \dot{q}_3 = q_4 \\ \dot{q}_4 = \kappa_4 q_2 + \kappa_5 q_3 + \kappa_6 q_4 + \gamma_2 \delta + \omega_2 \end{cases} \tag{11}$$

where

$$\begin{aligned} \kappa_1 &= -2\left(C_f + C_r\right)/m v_x, \quad \kappa_2 = -v_x \kappa_1, \\ \kappa_3 &= -2\left(C_f d_f - C_r d_r\right)/m v_x, \\ \gamma_1 &= 2C_f/m, \kappa_4 = -2\left(C_f d_f - C_r d_r\right)/J v_x, \\ \kappa_5 &= -v_x \kappa_4, \quad \kappa_6 = -2\left(C_f d_f^2 + C_r d_r^2\right)/J v_x, \\ \gamma_2 &= 2C_f d_f/J, \\ \omega_1 &= g\, sin(\theta_b) + \frac{\tilde{F}_{fy} + \tilde{F}_{ry}}{m} - (v_x - \kappa_3)\dot{\varphi}_d, \\ \omega_2 &= \frac{d_f \tilde{F}_{fy} - d_r \tilde{F}_{ry}}{J} + \kappa_6 \dot{\varphi}_d - \ddot{\varphi}_d. \end{aligned}$$

System (10) , (11) can be represented in the following form

$$\begin{cases} \dot{x}_1 = x_2 \\ \dot{x}_2 = f_1(x, z, t) + g_1(x, z, t)\delta \end{cases} \tag{12}$$

$$\begin{cases} \varepsilon \dot{z}_1 = z_2 \\ \varepsilon \dot{z}_2 = f_2(x, z, t) + g_2(x, z, t)\delta \end{cases} \tag{13}$$

We write the lateral dynamics in standard two-time scales form as follows:

$$\dot{X} = F_1(X, Z, t, \delta) \tag{14}$$

$$\varepsilon \dot{Z} = F_2(X, Z, t, \delta) \tag{15}$$

where

$$F_1(X, Z, t, \delta) = \begin{bmatrix} x_2 \\ \kappa_1 x_2 + \kappa_2 z_1 + \kappa_3 z_2 + \gamma_1 \delta \end{bmatrix} \tag{16}$$

$$F_2(X, Z, t, \delta) = \begin{bmatrix} z_2 \\ \kappa_4 x_2 + \kappa_5 z_1 + \kappa_6 z_2 + \gamma_2 \delta \end{bmatrix} \tag{17}$$

In step-1 and step-2, we determine the quasi-steady-state model and boundary layer model for lateral dynamics.

Step-1: We assume that the $\delta = u_s + u_f$ where u_s represents the input of slow subsystem while u_f denotes the input of fast subsystem:

$$\dot{X} = F_1\left(X, Z, t, u_s + u_f\right) \tag{18}$$

$$\varepsilon \dot{Z} = F_2\left(X, Z, t, u_s + u_f\right) \tag{19}$$

To determine the quasi-steady-state model, let $\varepsilon = 0$ and assume that $u_f = 0$ therefore,

$$\dot{X} = F_1(X, Z, t, u_s) \tag{20}$$
$$0 = F_2(X, Z, t, u_s) \tag{21}$$

Solving algebraic equation $F_2(X, Z, t, u_s) = 0$

$$\begin{bmatrix} z_2 \\ \kappa_4 x_2 + \kappa_5 z_1 + \kappa_6 z_2 + \gamma_2 u \end{bmatrix} = \begin{bmatrix} 0 \\ 0 \end{bmatrix} \tag{22}$$

It results in

$$\begin{bmatrix} z_1 \\ z_2 \end{bmatrix} = \begin{bmatrix} \frac{(-\kappa_4 x_2 - \gamma_2 u_s)}{\kappa_5} \\ 0 \end{bmatrix} \equiv \begin{bmatrix} h_1(x, t, u_s) \\ h_2(x, t, u_s) \end{bmatrix} \equiv H(x, t, u_s) \tag{23}$$

Now, solving $\dot{X} = F_1(X, H(x, t, u_s), t, u_s)$ and inserting disturbance $w_1(x, t)$,

$$\begin{bmatrix} \dot{x}_1 \\ \dot{x}_2 \end{bmatrix} = \begin{bmatrix} x_2 \\ \left(\kappa_1 - \frac{\kappa_2 \kappa_4}{\kappa_5}\right) x_2 + \left(\gamma_1 - \frac{\kappa_2}{\kappa_5}\gamma_2\right) u_s + w_1(x, t) \end{bmatrix} \equiv \begin{bmatrix} x_2 \\ f_1' + g_1' u_s + w_1(x, t) \end{bmatrix} \tag{24}$$

where,

$$f_1' = \left(\kappa_1 - \frac{\kappa_2 \kappa_4}{\kappa_5}\right) x_2; \quad g_1' = \gamma_1 - \frac{\kappa_2}{\kappa_5}\gamma_2$$

The system mentioned in (24) gives the quasi-steady-state model.

Step-2: To determine the boundary layer model, we define the error between desired manifold H and fast states Z as follows:

$$Y = Z - H(x, t, u_s) \tag{25}$$
$$\begin{bmatrix} y_1 \\ y_2 \end{bmatrix} = \begin{bmatrix} z_1 - h_1(x, t, u_s) \\ z_2 - h_2(x, t, u_s) \end{bmatrix} \tag{26}$$
$$\begin{bmatrix} y_1 \\ y_2 \end{bmatrix} = \begin{bmatrix} z_1 + \frac{\kappa_4}{\kappa_5} x_2 + \frac{\gamma_2}{\kappa_5} u_s \\ z_2 \end{bmatrix} \tag{27}$$
$$\begin{bmatrix} \varepsilon y_1 \\ \varepsilon y_2 \end{bmatrix} = \begin{bmatrix} \varepsilon z_1 + \varepsilon \frac{\kappa_4}{\kappa_5} x_2 + \varepsilon \frac{\gamma_2}{\kappa_5} u_s \\ \varepsilon z_2 \end{bmatrix} \tag{28}$$
$$\begin{bmatrix} \varepsilon \dot{y}_1 \\ \varepsilon \dot{y}_2 \end{bmatrix} = \begin{bmatrix} \varepsilon \dot{z}_1 + \varepsilon \frac{\kappa_4}{\kappa_5} \dot{x}_2 + \varepsilon \frac{\gamma_2}{\kappa_5} \dot{u}_s \\ \varepsilon \dot{z}_2 \end{bmatrix} \tag{29}$$
$$\begin{bmatrix} \varepsilon \dot{y}_1 \\ \varepsilon \dot{y}_2 \end{bmatrix} = \begin{bmatrix} z_2 + \varepsilon \frac{\kappa_4}{\kappa_5} \dot{x}_2 + \varepsilon \frac{\gamma_2}{\kappa_5} \dot{u}_s \\ \kappa_4 x_2 + \kappa_5 z_1 + \kappa_6 z_2 + \gamma_2 (u_s + u_f) \end{bmatrix} \tag{30}$$

Plugging in $z_1 = y_1 + h_1(x, t, u_s)$; $z_2 = y_2$

$$\begin{bmatrix} \varepsilon \dot{y}_1 \\ \varepsilon \dot{y}_2 \end{bmatrix} = \begin{bmatrix} y_2 + \varepsilon \frac{\kappa_4}{\kappa_5} \dot{x}_2 + \varepsilon \frac{\gamma_2}{\kappa_5} \dot{u}_s \\ \kappa_4 x_2 + \kappa_5 (y_1 + h_1(x, t, u_s)) + \kappa_6 y_2 + \gamma_2 (u_s + u_f) \end{bmatrix} \tag{31}$$

For $\varepsilon \approx 0$, the system is left with

$$\begin{bmatrix} \varepsilon \dot{y}_1 \\ \varepsilon \dot{y}_2 \end{bmatrix} = \begin{bmatrix} y_2 \\ \kappa_4 x_2 + \kappa_5 y_1 - \kappa_4 x_2 - \gamma_2 u_s + \kappa_6 y_2 + \gamma_2 u_s + \gamma_2 u_f \end{bmatrix} \tag{32}$$

Simplifying and inserting disturbance term $w_2(x, t)$,

$$\begin{bmatrix} \varepsilon \dot{y}_1 \\ \varepsilon \dot{y}_2 \end{bmatrix} = \begin{bmatrix} y_2 \\ \kappa_5 y_1 + \kappa_6 y_2 + \gamma_2 u_f + w_2(x, t) \end{bmatrix} \equiv \begin{bmatrix} y_2 \\ f_2' + g_2' u_s + w_2(x, t) \end{bmatrix} \tag{33}$$

where, $f_2' = \kappa_5 y_1 + \kappa_6 y_2$; $g_2' = \gamma_2$.

The system mentioned in (33) gives the boundary layer model.

IV. CONTROLLER DESIGN

In this section control law is devised for a two-time scale system of (24) and (33). The composite control is designed for a two-time scale system. This control law comprises two control signals that are designed for fast and slow systems mentioned in (24) and (33), respectively. In the proceeding text, fixed time SMC with barrier function is designed for first for quasi-steady-state model and then for boundary layer model.

To design the fixed settling time SMC with barrier function, consider the following linear sliding surfaces for slow and fast systems, respectively.

$$S_1 = a_1 x_1 + x_2 \tag{34}$$
$$S_2 = a_2 y_1 + y_2 \tag{35}$$

Assumption 2 ([51]): Initial condition for the output states, x_1 and y_1 ensures $|x_1(0)| < \hbar_1$ and $|y_1(0)| < \hbar_2$.

Assumption 3 ([59]): There exists a known upper bound $\omega(x)$ on the modeling uncertainties and disturbances. i.e., $w_i(t, x) \leq \omega(x)$; $i = 1, 2$.

Theorem 1: Under Assumption 1-3 the system (24) and (33) and the sliding manifolds (34)-(35) the control input $\delta = u_s + u_f$ guarantees the fixed settling time stabilization where,

$$u_s = -\frac{1}{g_1'} \left(\begin{array}{l} a_1 x_2 + f_1' + \omega_1 + \left(\frac{x_1 x_2}{\hbar_1^2 - x_1^2}\right) sign(S_1) \\ + sign(S_1) \begin{bmatrix} \alpha \left(|S_1| + \frac{0.5 x_1^2}{\hbar_1^2 - x_1^2}\right)^{\frac{1}{2}} \\ + \beta \left(|S_1| + \frac{0.5 x_1^2}{\hbar_1^2 - x_1^2}\right)^{\frac{3}{2}} \end{bmatrix} \end{array} \right) \tag{36}$$

and

$$u_f = -\frac{1}{g_2'}\left(\begin{array}{l} a_2y_2 + f_2' + \omega_2 + \left(\dfrac{y_1y_2}{\hbar_2^2 - y_1^2}\right)\text{sign}\,(S_2) \\ + \text{sign}\,(S_2)\left[\begin{array}{l} \alpha\left(|S_2| + \dfrac{0.5y_1^2}{\hbar_2^2 - y_1^2}\right)^{\frac{1}{2}} \\ +\beta\left(|S_2| + \dfrac{0.5y_1^2}{\hbar_2^2 - y_1^2}\right)^{\frac{3}{2}} \end{array}\right] \end{array}\right) \tag{37}$$

with $\alpha, \beta > 0$; $0 < p < 1$ and $q > 1$ and scalar constants $a_1, a_2 > 0$. sign (.) is defined as

$$\text{sign}\,(\eta) = \begin{cases} -1 & \eta < 0 \\ 1 & \eta \geq 0 \end{cases}$$

Moreover, for $\mathcal{B} \in \mathbb{R}^+$, $\hbar_1 < \mathcal{B}$ and $\hbar_2 < \mathcal{B}$ are chosen such that $|x_1(0)| < \hbar_1$ and $|z_1(0)| < \hbar_2$ then the output will satisfy the bound $|y(t)| < \mathcal{B} \forall t \geq 0$.

Proof: Let us define the following Lyapunov functions V_1 and V_2 in slow and fast time scales, respectively:

$$V_1 = |S_1| + \frac{1}{2} ln\left(\frac{\hbar_1^2}{\hbar_1^2 - x_1^2}\right) \tag{38}$$

$$V_2 = \varepsilon |S_2| + \varepsilon \frac{1}{2} ln\left(\frac{\hbar_2^2}{\hbar_2^2 - y_1^2}\right) \tag{39}$$

where S_1 and S_2 are sliding surfaces, defined by (34) and (35) and ε is the time scale parameter of the system. To prove the Theorem 1, we first show the convergence of slow and fast systems under separate controllers. Then we show that the outputs remain bounded for all time if they start within the bound. Finally, the fixed settling time convergence is proven.

A. SLOW CONTROLLER

By differentiating the Lyapunov function (38) we get

$$\dot{V}_1 = \dot{S}_1 \text{sign}\,(S_1) + \frac{x_1\dot{x}_1}{\hbar_1^2 - x_1^2}$$

$$\dot{V}_1 = \text{sign}\,(S_1)\left(a_1x_2 + f_1' + w_1 + g_1'u_s + \omega\right) + \frac{x_1x_2}{\hbar_1^2 - x_1^2}$$

By employing control law u_s given in (36)

$$\dot{V}_1 = \text{sign}\,(S_1)\left(\begin{array}{l} a_1x_2 + f_1' + w_1 \\ + g_1'\left(-\dfrac{1}{g_1'}\left(\begin{array}{l} a_1x_2 + f_1' + \omega_1 \\ + \left(\dfrac{x_1x_2}{\hbar_1^2 - x_1^2}\right) sign\,(S_1) \\ + sign\,(S_1)\left[\alpha\left(|S_1| + \dfrac{0.5x_1^2}{\hbar_1^2 - x_1^2}\right)^{\frac{1}{2}}\right. \\ \left. + \beta\left(|S_1| + \dfrac{0.5x_1^2}{\hbar_1^2 - x_1^2}\right)^{\frac{3}{2}}\right] \end{array}\right) + \omega_1\right) \\ + \dfrac{x_1x_2}{\hbar_1^2 - x_1^2} \end{array}\right)$$

By employing *Assumption-3*

$$\dot{V}_1 \leq \alpha\left(|S_1| + \frac{0.5x_1^2}{\hbar_1^2 - x_1^2}\right)^{\frac{1}{2}} + \beta\left(|S_1| + \frac{0.5x_1^2}{\hbar_1^2 - x_1^2}\right)^{\frac{3}{2}}$$

$$\dot{V}_1 \leq \alpha V_1^{1/2} + \beta V_1^{3/2} \tag{40}$$

B. FAST CONTROLLER

By differentiating the Lyapunov function (39) we get

$$\dot{V}_2 = \left(\varepsilon a_2\dot{y}_1 + \varepsilon\dot{y}_2\right)\text{sign}\,(S_2) + \frac{\varepsilon y_1\dot{y}_1}{\hbar_2^2 - y_1^2}$$

$$\dot{V}_2 = \left(a_2y_2 + f_2' + w_2 + g_2'u_f\right)\text{sign}\,(S_2) + \frac{y_1y_2}{\hbar_2^2 - y_1^2}$$

By employing control law u_f given in (37)

$$\dot{V}_2 = \left(\begin{array}{l} a_2y_2 + f_2' + w_2 + g_2'\left(-\dfrac{1}{g_2'}\right. \\ \times \left(\begin{array}{l} a_2y_2 + f_2' + \omega_2 \\ + \left(\dfrac{y_1y_2}{\hbar_2^2 - y_1^2}\right)\text{sign}\,(S_2) \\ + \text{sign}\,(S_2)\left[\alpha\left(|S_2| + \dfrac{0.5y_1^2}{\hbar_2^2 - y_1^2}\right)^{\frac{1}{2}}\right. \\ \left. + \beta\left(|S_2| + \dfrac{0.5y_1^2}{\hbar_2^2 - y_1^2}\right)^{\frac{3}{2}}\right] \end{array}\right) \\ \left.\times \text{sign}\,(S_2) + \dfrac{y_1y_2}{\hbar_2^2 - y_1^2}\right) \end{array}\right)$$

By employing *Assumption-3*,

$$\dot{V}_2 \leq \alpha\left(|S_2| + \frac{0.5y_1^2}{\hbar_2^2 - y_1^2}\right)^{\frac{1}{2}} + \beta\left(|S_2| + \frac{0.5y_1^2}{\hbar_2^2 - y_1^2}\right)^{\frac{3}{2}}$$

$$\dot{V}_2 \leq \alpha V_2^{1/2} + \beta V_2^{3/2} \tag{41}$$

By (40-41) u_s and u_f stabilize the slow and fast subsystems, therefore, by Tikhonov's theorem the composite control $u = u_s + u_f$ must stabilize the system (24) [65].

C. OUTPUT BOUNDEDNESS

Since $\dot{V}_i(t) < 0$ for $i = 1, 2$ it is deduced that $V_i(t) \leq V_{i0}$, where $V_{i0} = V_i(t = 0)$ that results in

$$|\xi_2 + a\xi_1| + \frac{1}{2} ln\left(\frac{\hbar_i^2}{\hbar_i^2 - \xi_1^2}\right) \leq V_{i0}$$

where $\xi = [x, y]$. Considering the second term only,

$$\frac{1}{2} ln \left(\frac{\hbar_i^2}{\hbar_i^2 - \xi_1^2} \right) \leq V_{i0}$$

Taking exponentials on both sides of inequality

$$\left(\frac{\hbar_i^2}{\hbar_i^2 - \xi_1^2} \right) \leq e^{2V_{i0}}$$

Note that, $\left(\hbar_i^2 - \xi_1^2\right) > 0 \forall t$ because of the condition $\xi_1(0) < \hbar_i$. We multiply this term on both sides of inequality

$$\hbar_i^2 \leq e^{2V_{i0}} \left(\hbar_i^2 - \xi_1^2\right)$$

This simplifies to

$$\xi_1^2 e^{2V_{i0}} \leq \hbar_i^2 \left(e^{2V_{i0}} - 1\right)$$

Dividing $e^{2V_{i0}}$ on both sides

$$\xi_1^2 \leq \hbar_i^2 \left(1 - \frac{1}{e^{2V_{i0}}}\right)$$

This inequality leads to

$$|\xi_1| \leq \hbar_i \sqrt{\left(1 - e^{-2V_{i0}}\right)}$$

Since by property of Lyapunov function $V_{i0} > 0$ and keeps a finite value, therefore $\sqrt{\left(1 - e^{-2V_{i0}}\right)} < 1$ and hence,

$$|\xi_1| < \hbar_i \quad \forall t \geq 0 \tag{42}$$

Therefore, the boundedness of outputs is established.

D. FIXED SETTLING TIME CONVERGENCE OF CONTROLLER

By Polyakov's definition of fixed time stability, (40-41) show that trajectories converge to corresponding sliding manifolds in fixed time. Once sliding mode is attained, the construction of sliding manifold guarantees exponential stability and hence, the convergence of outputs to ρ error bound in fixed time require only the maxima of output at time when $S_i = 0$ is established. The upper bound of outputs has been established in (42). Consequently, the fixed settling time stability of (24) under state feedback control law of Theorem 1 is guaranteed.

Corollary 1: The upper bound T on fixed settling time under state feedback control law of Theorem 1 is:

$$T < \frac{\pi}{\sqrt{\alpha\beta}} + \frac{1}{a_1} ln \left(\frac{\hbar_1}{\rho_1} \right) + \frac{\epsilon}{a_2} ln \left(\frac{\hbar_2}{\rho_2} \right)$$

Proof: First, we evaluate the reaching time T_r

$$\dot{V}_1 \leq -\alpha V_1^{\frac{1}{2}} - \beta V_1^{\frac{3}{2}}$$

By change of variable $V_1 = \omega^2$

$$2\omega\dot{\omega} \leq -\alpha\omega - \beta\omega^3$$

Simplifying the above expression,

$$2\frac{d\omega}{dt} \leq -\left(\alpha + \beta\omega^2\right)$$

Rearranging the terms in above expression

$$2\frac{d\omega}{\alpha + \beta\omega^2} \leq -dt$$

Integrating both sides of inequality

$$\begin{aligned} t &\leq -2 \int \frac{1}{\alpha + \beta\omega^2} d\omega \\ t &\leq -\frac{2}{\alpha} \int \frac{d\omega}{1 + \frac{\beta}{\alpha}\omega^2} \\ t &\leq -\frac{2}{\alpha}\sqrt{\frac{\alpha}{\beta}} \left[tan^{-1} \left(\sqrt{\frac{\beta}{\alpha}}\omega \right) - tan^{-1} \left(\sqrt{\frac{\beta}{\alpha}}\omega_0 \right) \right] \end{aligned}$$

After $t = T_r$, $V_1 = 0$ therefore $\omega = 0$. Hence,

$$\begin{aligned} T_r &\leq -\frac{2}{\alpha}\sqrt{\frac{\alpha}{\beta}} \left[tan^{-1}(0) - tan^{-1} \left(\sqrt{\frac{\beta}{\alpha}}\omega_0 \right) \right] \\ T_r &\leq \frac{2}{\alpha}\sqrt{\frac{\alpha}{\beta}} \left[tan^{-1} \left(\sqrt{\frac{\beta}{\alpha}}\omega_0 \right) \right] \\ T_r &\leq 2\sqrt{\frac{1}{\alpha\beta}} \left[tan^{-1} \left(\sqrt{\frac{\beta}{\alpha}}\omega_0 \right) \right] \end{aligned}$$

Since, $tan^{-1} \left(\sqrt{\frac{\beta}{\alpha}}\omega_0 \right) \leq \frac{\pi}{2}$, therefore

$$\begin{aligned} T_r &\leq 2\frac{1}{\sqrt{\alpha\beta}} \left(\frac{\pi}{2} \right) \\ T_r &\leq \frac{\pi}{\sqrt{\alpha\beta}} \end{aligned} \tag{43}$$

Now we will evaluate the sliding time T_s i.e., the time for states to stabilize to the equilibrium point after reaching the sliding surface.

After $V_1 = 0$, $|s_1| = 0$ which means that

$$\dot{x}_1 = -a_1 x_1 \tag{44}$$

The solution of the above equation is $x_1 = x_{10}^* e^{-a_1 t}$, where x_{10}^* denotes the value of state x_1 when the state reaches the respective sliding manifold. As stated in Definition 2, we assume that $\rho\%$ error is acceptable. Now, we evaluate the maximum time in which states attain the $\rho\%$ error margin. First, the time τ_{s_1} required for x_1 to reach within $\rho_1\%$ error margin is calculated by

$$\frac{\rho_1}{x_{10}^*} = e^{-a_1 \tau_{s_1}}$$

Since, by definition, the maximum value that x_1 can have is given by:

$$\begin{aligned} x_{10}^* &\leq \hbar_1 \\ \tau_{s_1} &\leq -\frac{1}{a_1} ln \left(\frac{\rho_1}{\hbar_1} \right) \\ \tau_{s_1} &\leq \frac{1}{a_1} ln \left(\frac{\hbar_1}{\rho_1} \right) \end{aligned} \tag{45}$$

Similarly, the time τ_{s_2} required for z_1 to reach within $\rho_2\%$ error margin is calculated by

$$\frac{\rho_2}{z_{10}^*} = e^{-a_2\tau_{s_2}/\epsilon}$$

According to Theorem-1, the maximum value that z_1 can have is given by:

$$\begin{aligned} z_{10}^* &\leq \hbar_2 \\ \tau_{s_2} &\leq -\frac{\epsilon}{a_2} ln\left(\frac{\rho_2}{\hbar_2}\right) \\ \tau_{s_2} &\leq \frac{\epsilon}{a_2} ln\left(\frac{\hbar_2}{\rho_2}\right) \end{aligned} \tag{46}$$

This means that after being on the sliding manifold, the maximum time for states to reach to origin for these subsystems is:

$$\tau_{s_1} < \frac{1}{a_1} ln\left(\frac{\hbar_1}{\rho_1}\right) \text{ and } \tau_{s_2} < \frac{\epsilon}{a_2} ln\left(\frac{\hbar_2}{\rho_2}\right)$$

These are the sliding times required for slow and fast time scales, respectively.

Finally, the overall settling time T for the system (24) under state feedback control law of Theorem 1 would be

$$\begin{aligned} T &< T_R + \tau_{s_1} + \tau_{s_2} \\ T &< \frac{\pi}{\sqrt{\alpha\beta}} + \frac{1}{a_1} ln\left(\frac{\hbar_1}{\rho_1}\right) + \frac{\epsilon}{a_2} ln\left(\frac{\hbar_2}{\rho_2}\right) \end{aligned} \tag{47}$$

Note that, the settling time of this system is independent of the initial conditions of the system.

V. SIMULATION RESULTS

This section presents the CarSim and MATLAB-based simulation results for the DLC problem of the self-driving car. The DLC trajectory in accordance with ISO 3888-2 is obtained from CarSim and the proposed two-time scale model-based control (5) is implemented in MATLAB. The control input of the steering wheel angle is fed to CarSim and the resulting performance of the controller is studied. The block diagram to illustrate the signal flow in simulations is given in FIGURE 2.

The simulations are performed for E-Class Sedan (the dimensions and vehicle parameters are provided in Table-1) for different values of road friction coefficient at different longitudinal speeds. In section-3, the controller is designed to track a global yaw reference. In our simulations, the standard DLC trajectory is imported into MATLAB from CarSim. Later, the yaw reference is generated using this DLC trajectory by employing the following relation $\psi_d = \text{atan}\left[(X_n - X_{n-\tau}) \,/\, (Y_n - Y_{n-\tau})\right]$; where X_n and Y_n represent the current longitudinal and lateral position reference, respectively while $X_{n-\tau}$ and $Y_{n-\tau}$ respectively denote the τ-delayed longitudinal and lateral positions. τ defines the amount of delay and is assumed to be $\tau = 0.0005$ in our simulations. Moreover, the ODE8 solver is used with a fixed step size of 0.0001 in Simulink.

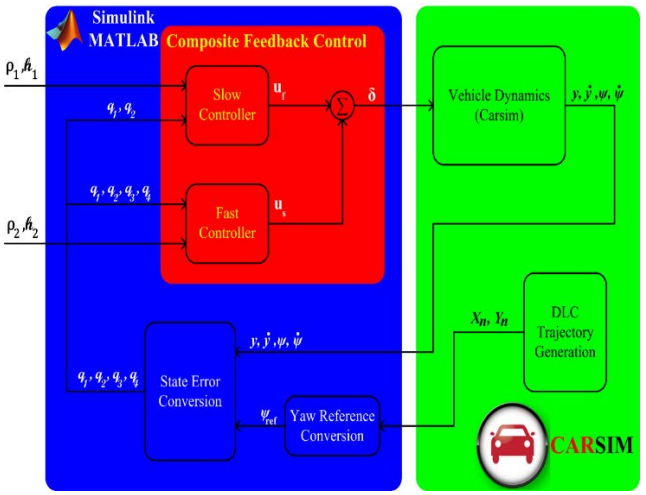

FIGURE 2. Illustration of simulation in CarSim and MATLAB.

For the implementation of the controller on the self-driving car, lateral position, lateral speed, yaw angle, and yaw rate are imported into Simulink from CarSim. The longitudinal speed v_x of the vehicle is fixed to 40 km/h, 45 km/h, 50 km/h and 55 km/h and results are discussed in the following paragraphs. Moreover, the road friction coefficient μ is also altered between 0.5 and 0.85 to evaluate the controller performance. The control law is implemented by setting $W = 3$ and $a = 2$. The limit of lateral position error $\hbar_1$ is set to $1.25m$ while that on yaw error is set to $\hbar_2 = 10°$. The allowable steady-state error margin $\rho = [\rho_1, \rho_2]$ is supposed to be $[0.5m, 1.5°]$ while $\alpha = \beta = 1$ and $\epsilon = 1$. These control parameters result in the fixed settling time of $T = 4.06s$. The simulation results for different longitudinal speeds and road friction are discussed below.

TABLE 1. E-class sedan vehicle parameters (CarSim).

Symbol	Description	Value
m	Mass of Vehicle	$1650kg$
g	Gravitational acceleration	$9.81\ m/s^2$
J	Yaw inertia	$3234kgm^2$
d_f	Front wheels distance from CG	$1.4\ m$
d_r	Rear wheels distance from CG	$1.65m$
C_f	Front Tire Cornering Stiffness	$75\ kN/rad$
C_r	Rear Tire Cornering Stiffness	$84kN/rad$

A. CASE-1 HIGH FRICTION SURFACE ($\mu = 0.85$)

In the following results, the road friction coefficient is fixed to 0.85 and the performance of the controller is studied by varying the longitudinal speed of the self-driving car. In all the cases, the same control parameters have been used that yield the maximum settling time of the controller to be 4.06s.

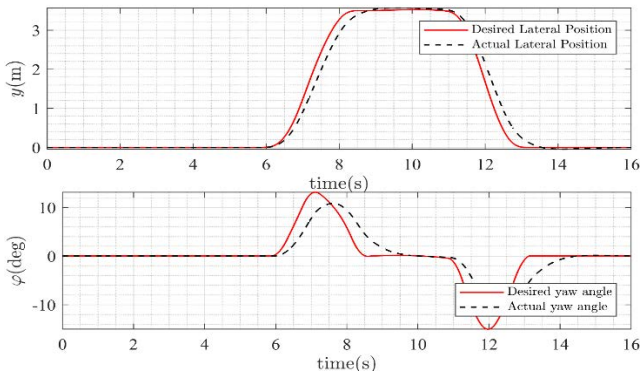

FIGURE 3. Tracking of lateral position and Yaw angle at $v_x = 40\,km/h$.

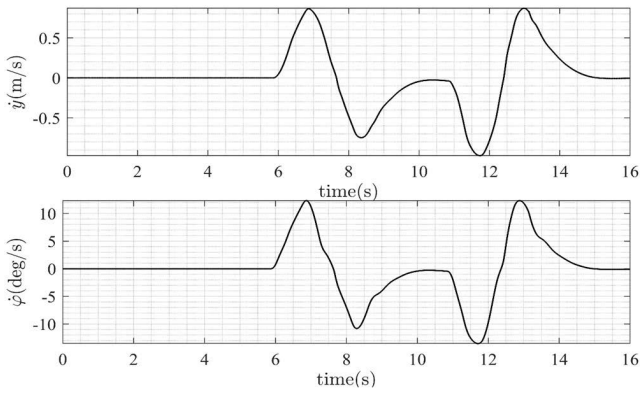

FIGURE 4. Lateral speed and Yaw rate at $v_x = 40\,km/h$.

1) $v_x = 40\,km/h$

In the simulation results of FIGURE 3 to FIGURE 8, the longitudinal speed of the self-driving car is fixed to $40\,km/h$. FIGURE 3 shows the tracking of lateral position and yaw angle. The results show that the designed controller shows acceptable performance for abruptly changing reference. The lateral speed and yaw rate are plotted in FIGURE 4. The graphs show that the rate of change eventually settles to zero after the second lane change. The plot of control (steering) input is shown in FIGURE 5. The highest magnitude of steering input required to accomplish DLC maneuver at $40\,km/h$ is $\delta = 77°$. The plot for DLC trajectory tracking upon the global axis is given in Figure 6. The error plots of lateral position e_1 and yaw e_3 are given in FIGURE 7 and FIGURE 8, respectively. Maximum errors are $e_1^{\text{MAX}} = 0.18$ and $e_3^{\text{MAX}} = 6.3°$ while maximum lateral speed and yaw rate errors are $\dot{e}_1^{\text{MAX}} = 0.31 m/s$ and $\dot{e}_3^{\text{MAX}} = 14°/s$. Note that after settling of states, the errors stay in nominated bound i.e. $e_1, e_3 < \rho$. Moreover, during transients, the constraints are also fulfilled i.e., $e_1 < \hbar_1$ and $e_3 < \hbar_2$.

2) $v_x = 45\,km/h$

In FIGURE 9 to FIGURE14, the v_x is set to $45\,km/h$. FIGURE 9 shows the tracking of lateral position and yaw angle. The results show that the reference y and ψ are tracked by CarSim dynamics using model-based control. The lateral

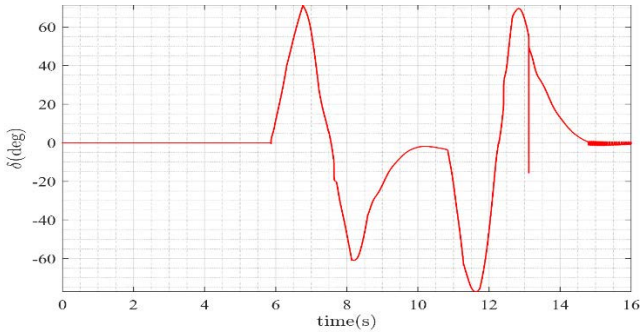

FIGURE 5. Steering angle at $v_x = 40\,km/h$.

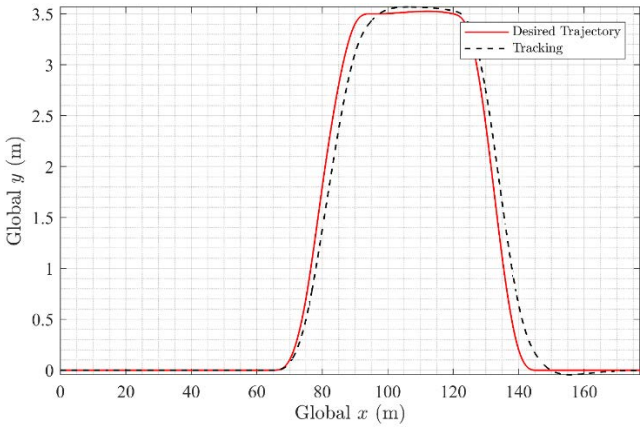

FIGURE 6. Trajectory tracking of self-driving car at $v_x = 40\,km/h$

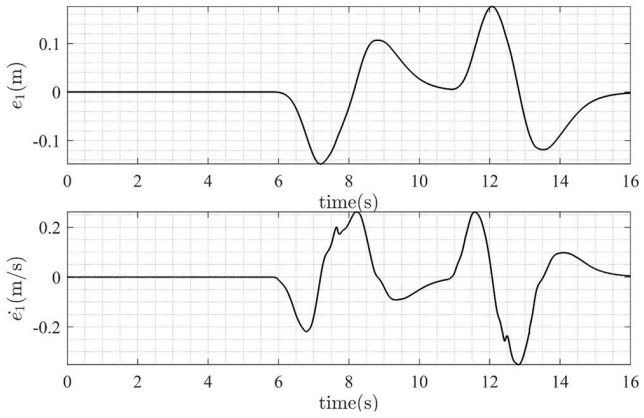

FIGURE 7. Lateral position and speed error at $v_x = 40\,km/h$.

speed and yaw rate are plotted in FIGURE 10. The graphs show that the rate of change eventually settles to zero after the second lane change. The plot of control (steering) input is shown in FIGURE 11. The highest magnitude of steering input required to accomplish DLC maneuver at $45\,km/h$ is $\delta = 85°$. Moreover, the chattering can be observed in δ as being drawback of sliding mode control. The plot for DLC trajectory tracking upon the global axis is given in FIGURE 12.

After following the path, the vehicle eventually sustains its forward motion at $y = 0$. The error plots of lateral

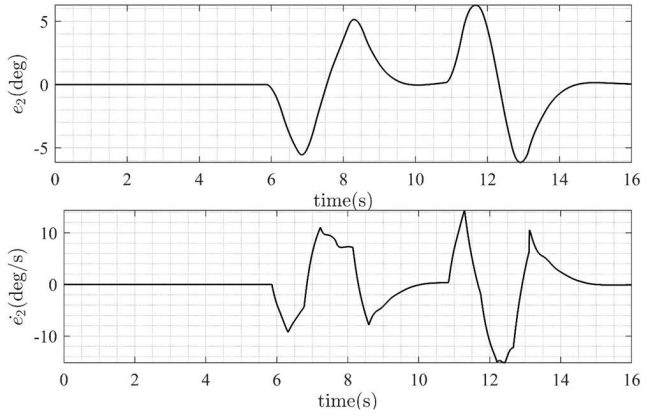

FIGURE 8. Yaw and Yaw rate error at $v_x = 40\,km/h$.

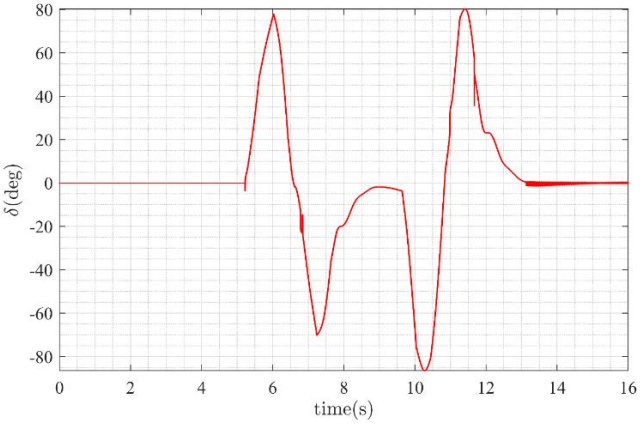

FIGURE 11. Steering angle at $v_x = 45\,km/h$.

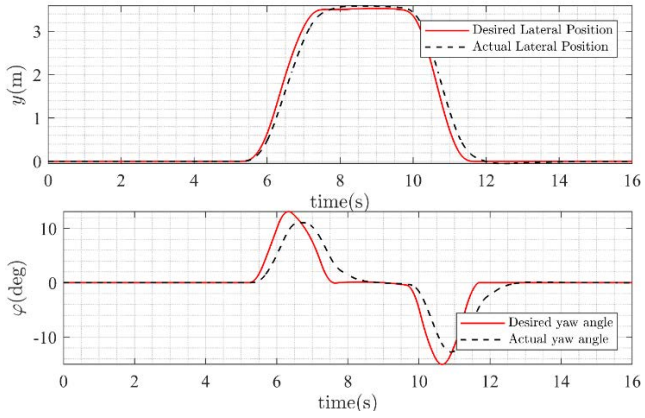

FIGURE 9. Tracking of lateral position and Yaw angle at $v_x = 45\,km/h$.

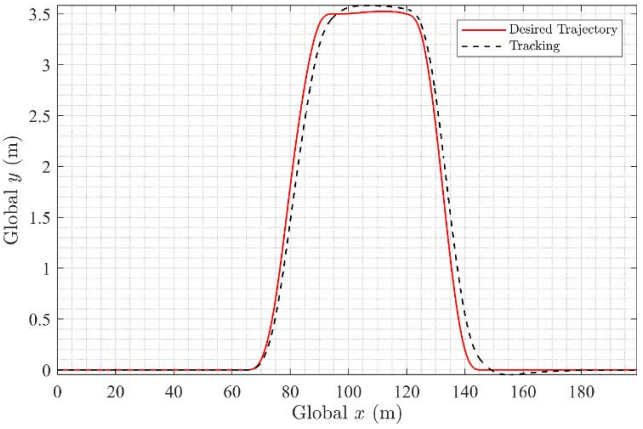

FIGURE 12. Trajectory tracking of self-driving car at $v_x = 45\,km/h$.

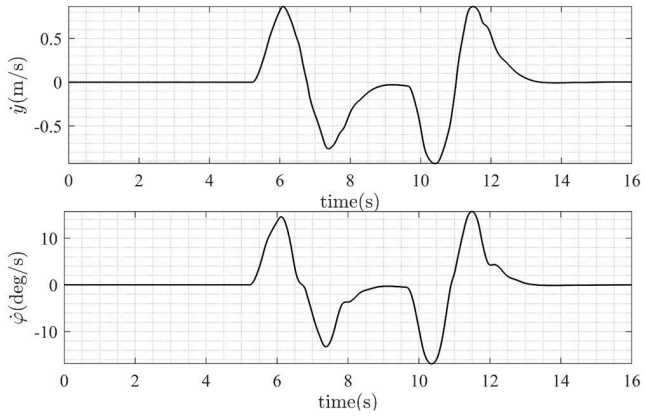

FIGURE 10. Lateral speed and Yaw rate at $v_x = 45\,km/h$.

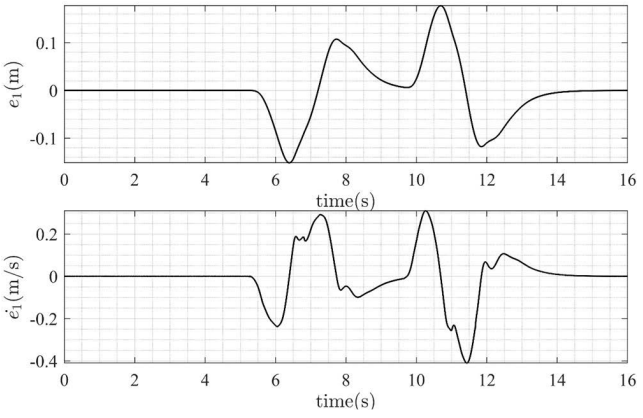

FIGURE 13. Lateral position and speed error at $v_x = 45\,km/h$.

position e_1 and yaw e_3 are given in FIGURE 13 and FIGURE 14, respectively. Maximum position errors are $e_1^{\text{MAX}} = 0.19$ and $e_3^{\text{MAX}} = 6°$, while maximum lateral speed and yaw rate errors are $\dot{e}_1^{\text{MAX}} = 0.41 m/s$ and $\dot{e}_3^{\text{MAX}} = 15°/s$. Note that after settling of states, the errors stay in nominated bound i.e. $e_1, e_3 < \rho$. Moreover, during transients, the constraints are also fulfilled i.e. $e_1 < \hbar_1$ and $e_3 < \hbar_2$.

3) $v_x = 50\,km/h$

In FIGURE 15 to FIGURE 20, the v_x is set to $50\,km/h$. FIGURE 15 shows the tracking of lateral position and yaw angle. The results show that the reference y and ψ are tracked by CarSim dynamics using model-based control. The lateral speed and yaw rate are plotted in FIGURE 16. The graphs show that the rate of change eventually settles to zero after

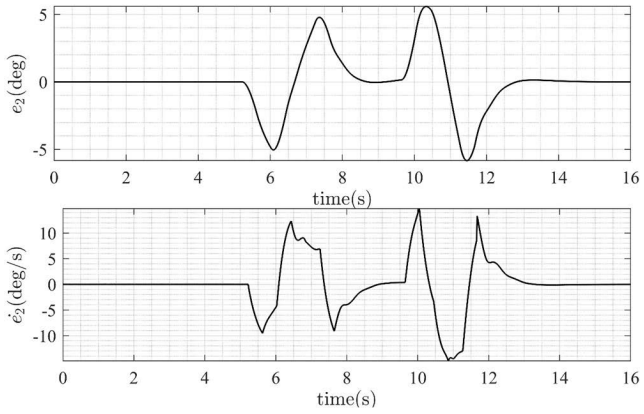

FIGURE 14. Yaw and Yaw rate error at $v_x = 45\,km/h$.

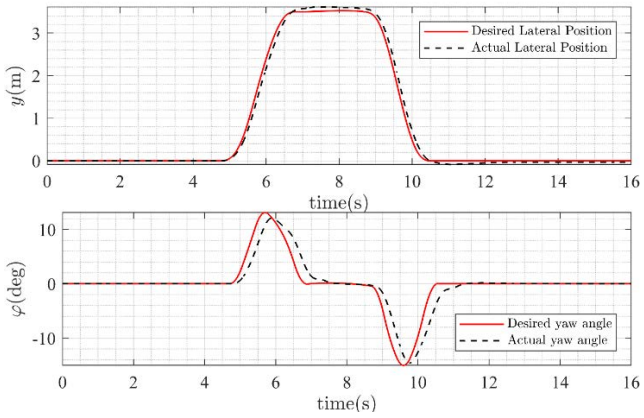

FIGURE 15. Tracking of lateral position and Yaw angle at $v_x = 50\,km/h$.

the second lane change. The plot of control (steering) input is shown in FIGURE 17. The highest magnitude of steering input required to accomplish DLC maneuver at $50\,km/h$ is $\delta = 106°$. Moreover, the chattering can be observed in δ as being drawback of sliding mode control. The plot for DLC trajectory tracking upon the global axis is given in FIGURE 18. After following the path, the vehicle eventually sustains its forward motion at $y = 0$. The error plots of lateral position e_1 and yaw e_3 are given in FIGURE 19 and FIGURE 20, respectively. Maximum position errors are $e_1^{\text{MAX}} = 0.2$ and $e_3^{\text{MAX}} = 6.2°$, while maximum lateral speed and yaw rate errors are $\dot{e}_1^{\text{MAX}} = 0.46\,m/s$ and $\dot{e}_3^{\text{MAX}} = 16°/s$, respectively. Note that after settling of states, the errors stay in nominated bound i.e. $e_1, e_3 < \rho$. Moreover, during transients, the constraints are also fulfilled i.e. $e_1 < \hbar_1$ and $e_3 < \hbar_2$. A steady state error of 0.03m is also induced in lateral position.

4) $v_x = 55km/h$

From FIGURE 21 to FIGURE 26, the v_x is set to $55\,km/h$. FIGURE 21 shows the tracking of lateral position and yaw angle. The results show that the reference y and ψ are tracked by CarSim dynamics using model-based control. The lateral speed and yaw rate are plotted in FIGURE 22. The graphs

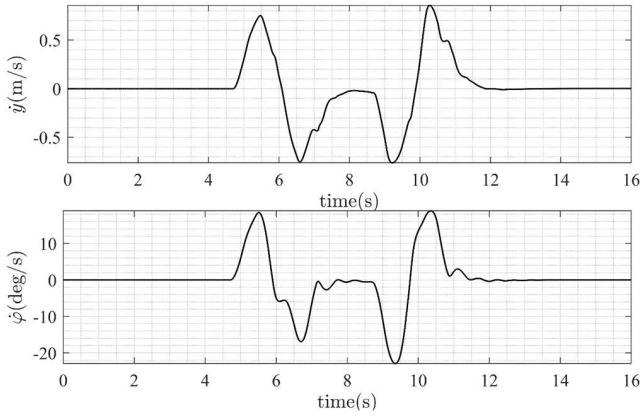

FIGURE 16. Lateral speed and Yaw rate at $v_x = 50\,km/h$.

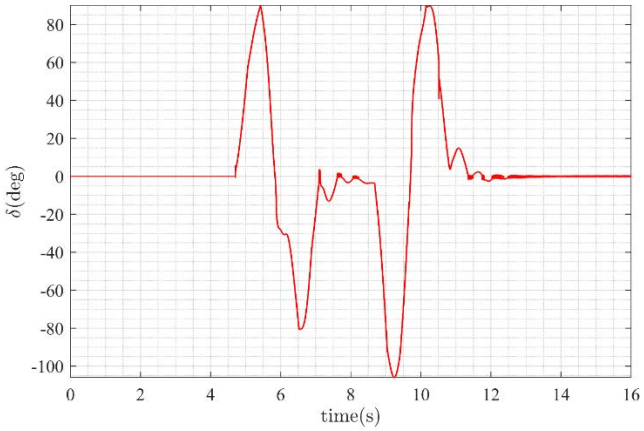

FIGURE 17. Steering angle at $v_x = 50\,km/h$.

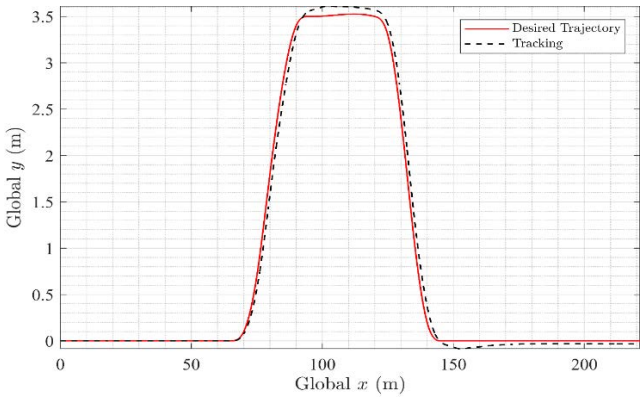

FIGURE 18. Trajectory tracking of self-driving car at $v_x = 50\,km/h$.

show that the rate of change eventually settles to zero after the second lane change.

The plot of control (steering) input is shown in FIGURE 23. The highest magnitude of steering input required to accomplish DLC maneuver at $55\,km/h$ is $\delta = 114°$. Moreover, the chattering can be observed in δ as being drawback of sliding mode control. The plot for DLC trajectory tracking upon the global axis is given

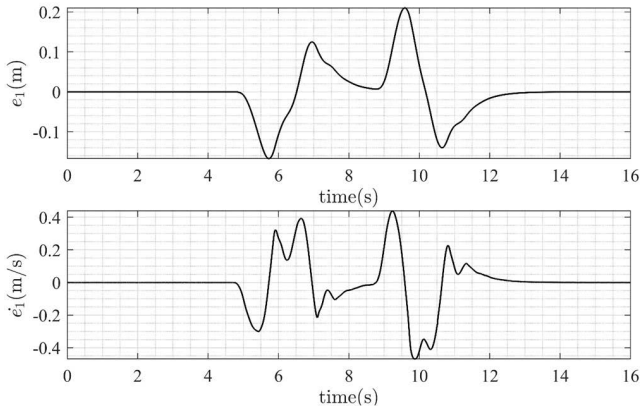

FIGURE 19. Lateral position and speed error at $v_x = 50\,km/h$.

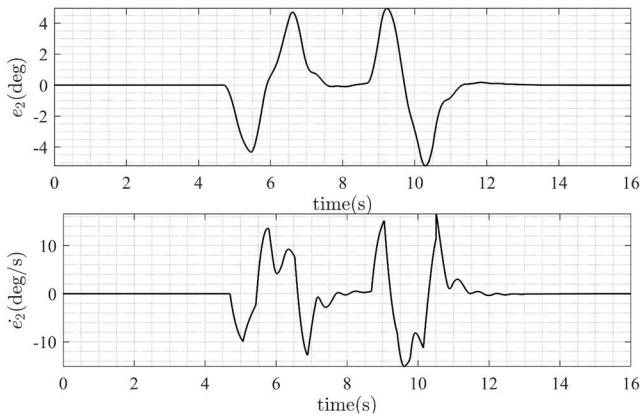

FIGURE 20. Yaw and Yaw rate error at $v_x = 50\,km/h$.

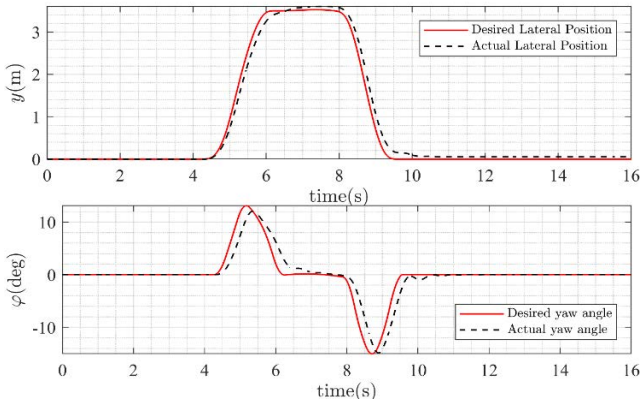

FIGURE 21. Tracking of lateral position and Yaw angle at $v_x = 55\,km/h$.

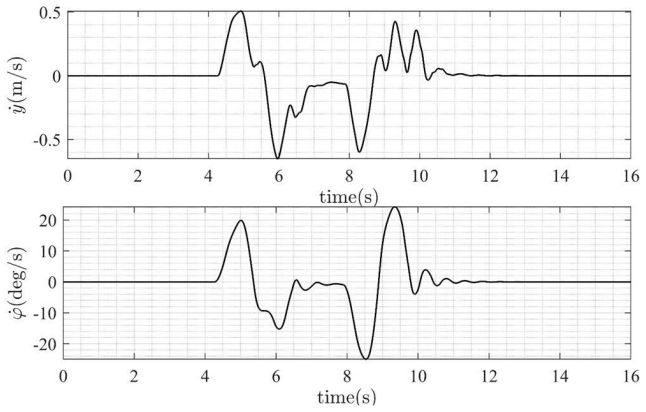

FIGURE 22. Lateral speed and Yaw rate at $v_x = 55\,km/h$.

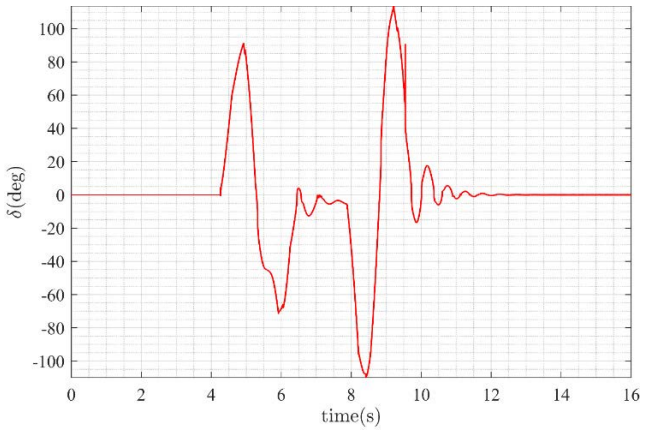

FIGURE 23. Steering angle at $v_x = 55\,km/h$.

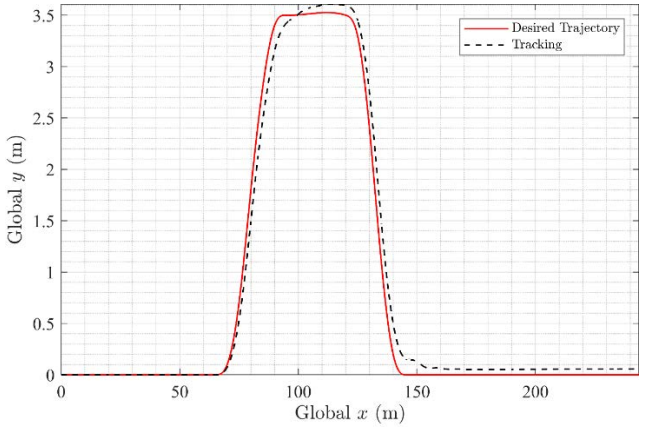

FIGURE 24. Trajectory tracking of self-driving car at $v_x = 50\,km/h$.

in FIGURE 24. After following the path, the vehicle eventually sustains its forward motion at $y \approx 0$. The error plots of lateral position e_1 and yaw e_3 are given in FIGURE 25 and FIGURE 26, respectively.

Maximum position errors are $e_1^{\text{MAX}} = 0.47$ and $e_3^{\text{MAX}} = 5.25°$, while maximum lateral speed and yaw rate errors are $\dot{e}_1^{\text{MAX}} = 0.95\,m/s$ and $\dot{e}_3^{\text{MAX}} = 19°/s$, respectively. Note that after settling of states, the errors stay in nominated bound i.e., $e_3 < \rho$. Moreover, during transients, the constraints are also fulfilled, i.e., $e_1 < \hbar_1$ and $e_3 < \hbar_2$. A steady-state error of $0.05m$ is also induced in lateral position i.e., $e_1 > \rho$ this is because of a very abrupt change in trajectory and the two-time scales controller cannot handle it.

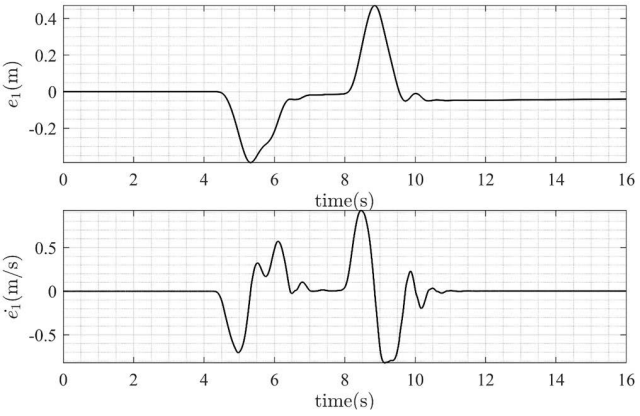

FIGURE 25. Lateral position and speed error at $v_x = 50\,km/h$.

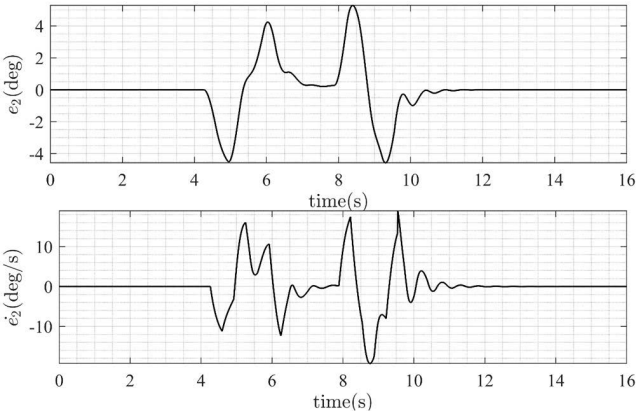

FIGURE 26. Yaw and Yaw rate error at $v_x = 55\,km/h$.

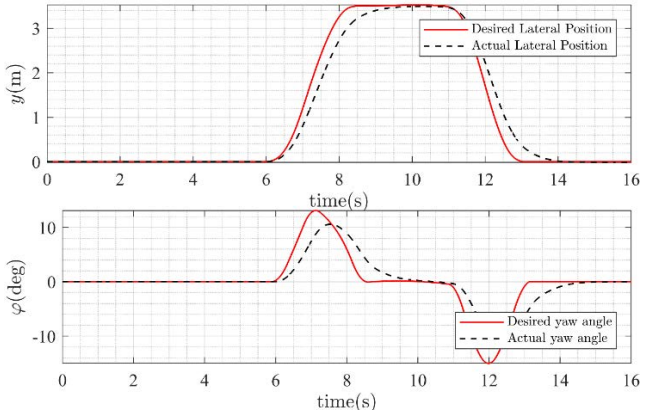

FIGURE 27. Tracking of lateral position and Yaw angle at $v_x = 40\,km/h$.

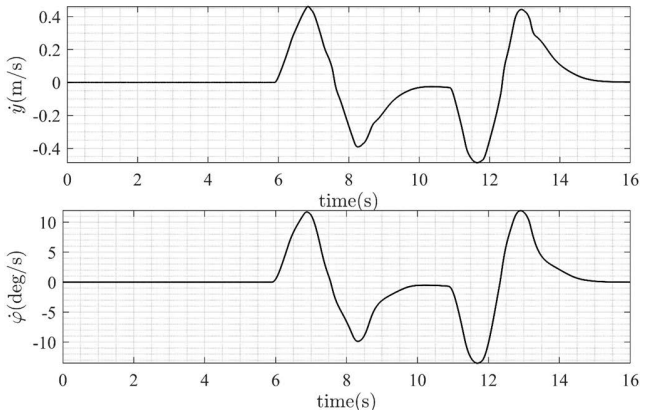

FIGURE 28. Lateral speed and Yaw rate at $v_x = 40\,km/h$.

B. CASE-2 LOW FRICTION SURFACE ($\mu = 0.5$)

1) $v_x = 40\,km/h$

In the simulation results of FIGURE 27 to FIGURE 32, the longitudinal speed of a self-driving vehicle is fixed to $40\,km/h$. FIGURE 27 shows the tracking of lateral position and yaw angle. Compared to the case of $\mu = 0.85$, the performance has been deteriorated here. The results show that the designed controller show acceptable performance for abruptly changing reference. The lateral speed and yaw rate are plotted in FIGURE 28. The graphs show that the rate of change eventually settles to zero after the second lane change. The plot of control (steering) input is shown in FIGURE 29. The highest magnitude of steering input required to accomplish DLC maneuver at $40\,km/h$ is $\delta = 85°$. Moreover, the chattering can be observed in δ as being drawback of sliding mode control. The plot for DLC trajectory tracking upon the global axis is given in FIGURE 30. After following the path, the vehicle eventually sustains its forward motion at $y = 0$. The error plots of lateral position e_1 and yaw e_3 are given in FIGURE 31 and FIGURE 32, respectively. Maximum errors are $e_1^{\text{MAX}} = 0.6$ and $e_3^{\text{MAX}} = 6.4°$ while maximum lateral speed and yaw rate errors are $\dot{e}_1^{\text{MAX}} = 0.73 m/s$ and $\dot{e}_3^{\text{MAX}} = 15°/s$. Note that after settling of states, the errors stay in nominated bound i.e., $e_1, e_3 < \rho$.

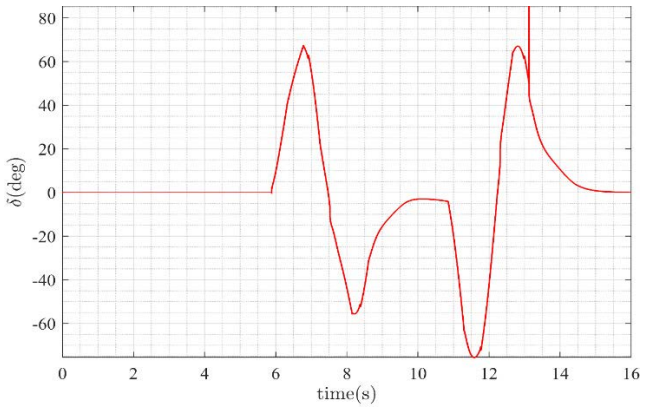

FIGURE 29. Steering angle at $v_x = 40\,km/h$.

Moreover, during transients, the constraints are also fulfilled i.e. $e_1 < \hbar_1$ and $e_3 < \hbar_2$.

2) $v_x = 45\,km/h$

In the simulation results of FIGURE 33 to FIGURE 38, the lateral speed of a self-driving car is fixed to $45\,km/h$. FIGURE 33 shows the tracking of lateral position and yaw angle. Compared to the case of $\mu = 0.85$, the performance has been deteriorated here.

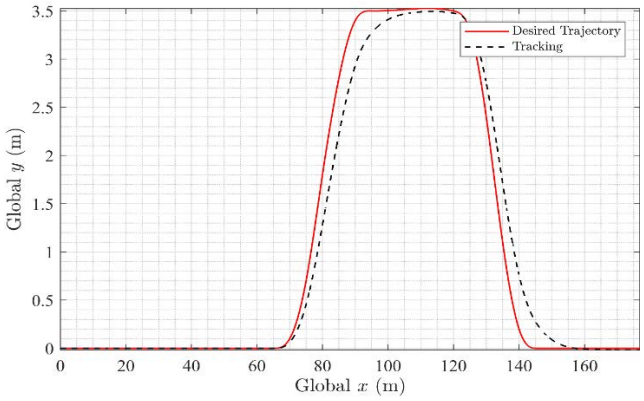

FIGURE 30. Trajectory tracking of self-driving car at $v_x = 40\,km/h$.

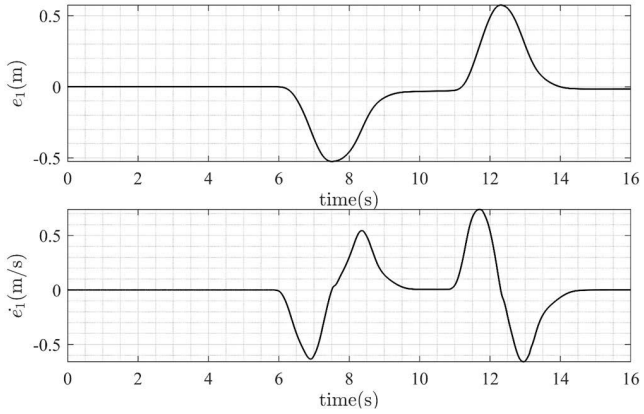

FIGURE 31. Lateral position and speed error at $v_x = 40\,km/h$.

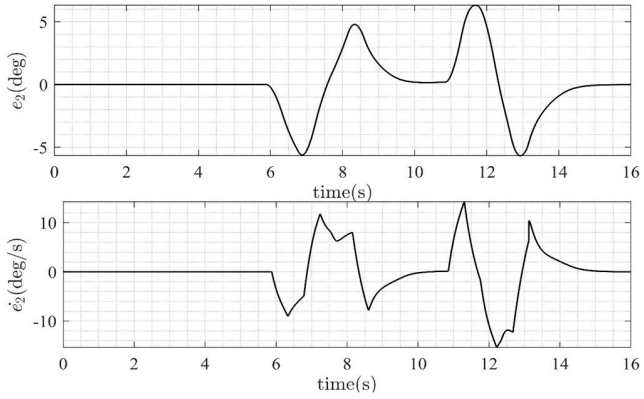

FIGURE 32. Yaw and Yaw rate error at $v_x = 40\,km/h$.

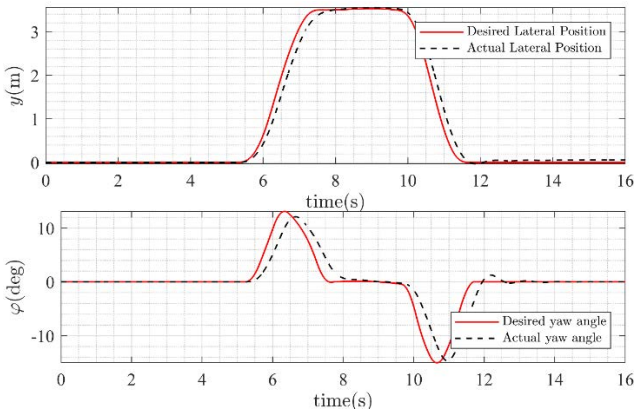

FIGURE 33. Tracking of lateral position and Yaw angle at $v_x = 45\,km/h$.

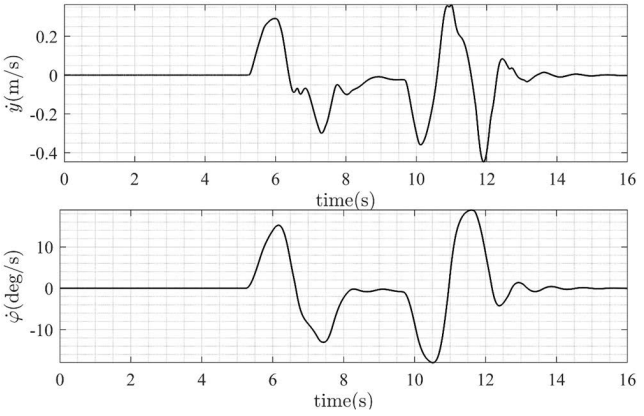

FIGURE 34. Lateral speed and Yaw rate at $v_x = 45\,km/h$.

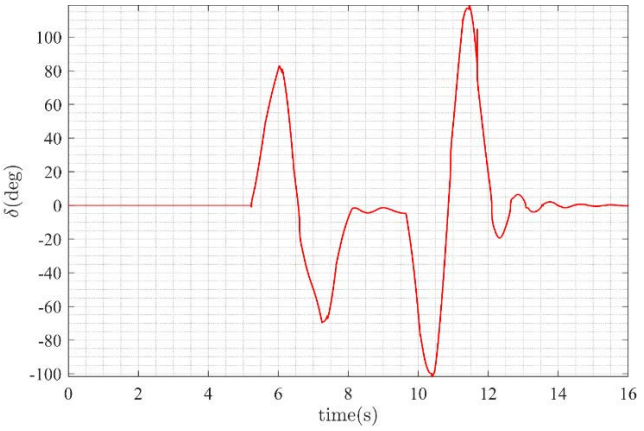

FIGURE 35. Steering angle at $v_x = 45 km/h$.

The results show that the designed controller shows acceptable performance for abruptly changing reference. The lateral speed and yaw rate are plotted in FIGURE 34. The graphs show that the rate of change eventually settles to zero after the second lane change. The plot of control (steering) input is shown in FIGURE 35. The highest magnitude of steering input required to accomplish DLC maneuver at $45\,km/h$ is $\delta = 120°$. Moreover, the chattering can be observed in δ as being drawback of sliding mode control. The plot for DLC trajectory tracking upon the global axis is given in FIGURE 36.

After following the path, the vehicle eventually sustains its forward motion at $y \approx 0$. The error plots of lateral position e_1 and yaw e_3 are given in FIGURE 37 and FIGURE 38, respectively. Maximum errors are $e_1^{MAX} = 0.72$ and $e_3^{MAX} = 6°$ while maximum lateral speed and yaw rate errors are $\dot{e}_1^{MAX} = 1.2 m/s$ and $\dot{e}_3^{MAX} = 20°/s$. Note that after settling of states, the errors stay in nominated bound

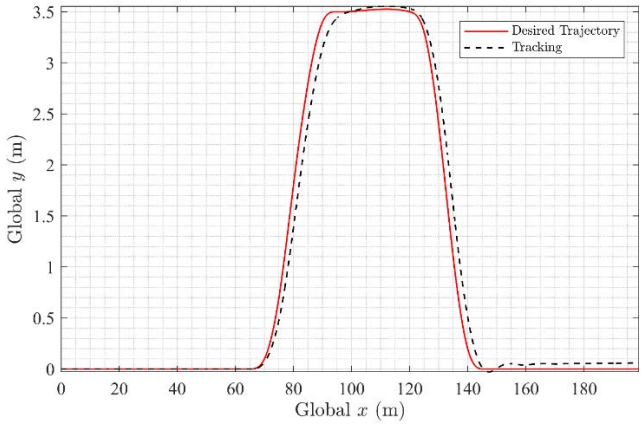

FIGURE 36. Trajectory tracking of self-driving car at $v_x = 45\,km/h$.

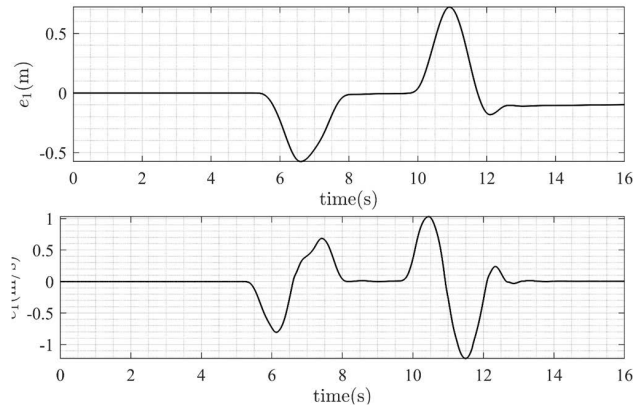

FIGURE 37. Lateral position and speed error at $v_x = 45\,km/h$.

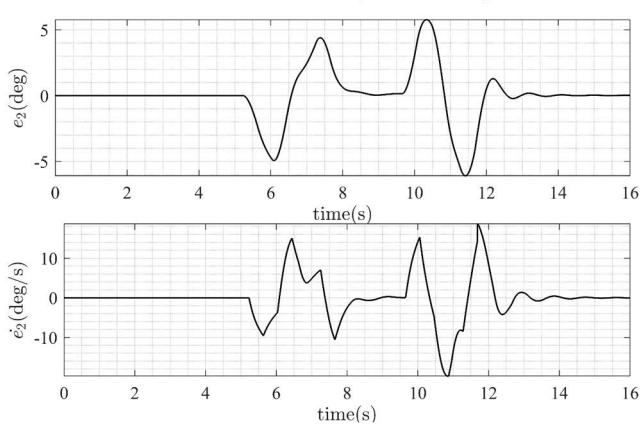

FIGURE 38. Yaw and Yaw Rate Error at $v_x = 45\,km/h$.

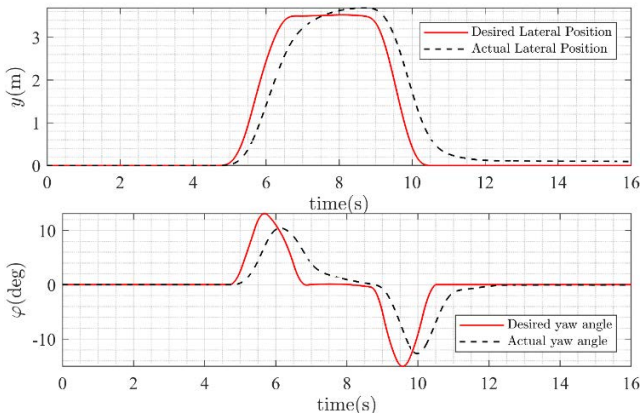

FIGURE 39. Tracking of lateral position and Yaw angle at $v_x = 50\,km/h$.

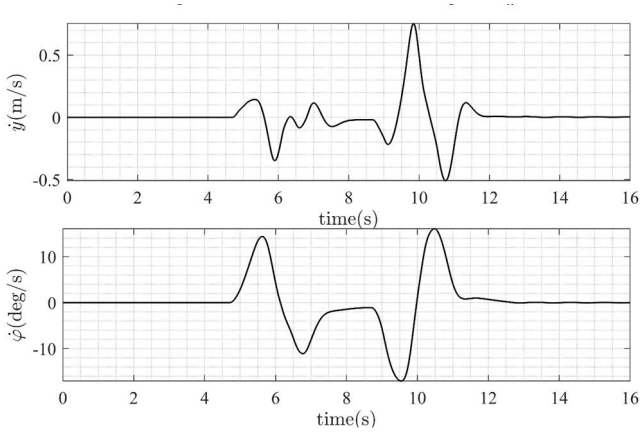

FIGURE 40. Lateral speed and Yaw rate at $v_x = 50\,km/h$.

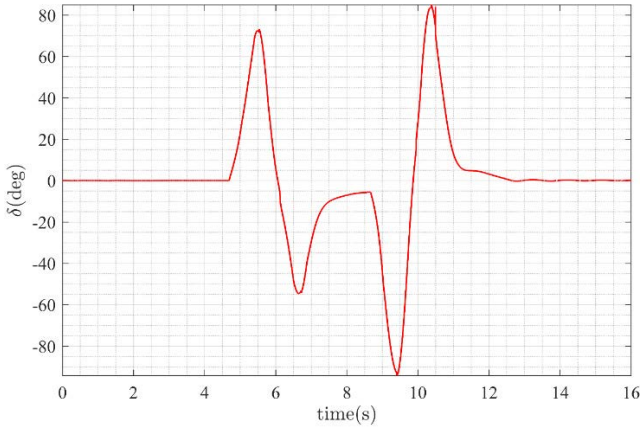

FIGURE 41. Steering angle at $v_x = 50\,km/h$.

i.e. $e_1, e_3 < \rho$. Moreover, during transients, the constraints are also fulfilled i.e. $e_1 < \hbar_1$ and $e_3 < \hbar_2$. Steady state error $e_1 = 0.07m$.

3) $v_x = 50km/h$

In the simulation results of FIGURE 39 to FIGURE 44, the longitudinal speed of a self-driving car is fixed to $50\,km/h$. FIGURE 39 shows the tracking of lateral position and yaw angle. Compared to the case of $\mu = 0.85$, the performance has been deteriorated here. The results show that that the designed controller show acceptable performance for abruptly changing reference. The lateral speed and yaw rate are plotted in FIGURE 40. The graphs show that the rate of change eventually settles to zero after the second lane change. The plot of control (steering) input is shown in FIGURE 41. The highest magnitude of steering input required to accomplish DLC maneuver at $50\,km/h$ is $\delta = 96°$. Moreover, the

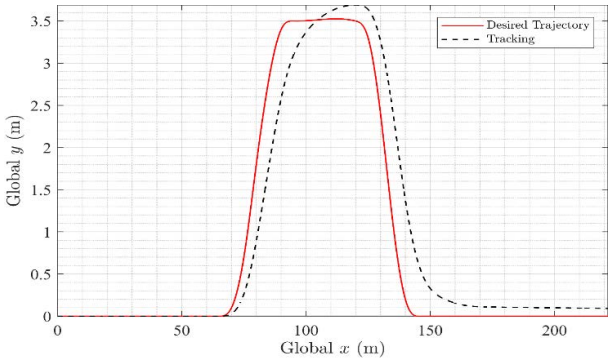

FIGURE 42. Trajectory tracking of self-driving Car at $v_x = 50\,km/h$.

chattering can be observed in δ as being drawback of sliding mode control. The plot for DLC trajectory tracking upon the global axis is given in FIGURE 42. After following the path, the vehicle eventually sustains its forward motion at $y \approx 0$. The error plots of lateral position e_1 and yaw e_3 are given in FIGURE 43 and FIGURE 44, respectively. Maximum errors are $e_1^{\text{MAX}} = 1.82m$ and $e_3^{\text{MAX}} = 8.5°$ while maximum lateral speed and yaw rate errors are $\dot{e}_1^{\text{MAX}} = 2.3m/s$ and $\dot{e}_3^{\text{MAX}} = 26°/s$. Note that after settling of states, the errors stay in nominated bound i.e., $e_1, e_3 < \rho$. Moreover, during transients, the constraints are also fulfilled i.e. $e_1 < \hbar_1$ and $e_3 < \hbar_2$.

4) $v_x = 55\,km/h$

In the simulation results of FIGURE 45 to FIGURE 50, the longitudinal speed of a self-driving car is fixed to $50\,km/h$. FIGURE 45 shows the tracking of lateral position and yaw angle. Compared to the case of $\mu = 0.85$, the performance has been deteriorated here. The results show that that the designed controller show acceptable performance for abruptly changing reference. The lateral speed and yaw rate are plotted in FIGURE 46. The graphs show that the rate of change eventually settles to zero after the second lane change. The plot of control (steering) input is shown in FIGURE 47 The highest magnitude of steering input required to accomplish DLC maneuver at $50\,km/h$ is $\delta = 162°$. Moreover, the chattering can be observed in δ as being drawback of sliding mode control. The plot for DLC trajectory tracking upon the global axis is given in FIGURE 48. After following the path, the vehicle eventually sustains its forward motion at $y \approx 0$.

The error plots of lateral position e_1 and yaw e_3 are given in FIGURE 49 and FIGURE 50, respectively. Maximum errors are $e_1^{\text{MAX}} = 1.9$ and $e_3^{\text{MAX}} = 12°$ while maximum lateral speed and yaw rate errors are $\dot{e}_1^{\text{MAX}} = 3m/s$ and $\dot{e}_3^{\text{MAX}} = 35°/s$. Note that after settling of states, the errors stay in nominated bound i.e. $e_1, e_3 < \rho$. Moreover, during transients, the constraints are also fulfilled i.e. $e_1 < \hbar_1$ and $e_3 < \hbar_2$.

C. FSTSMC PERFORMANCE FOR VARYING GAINS AT SAME INITIAL CONDITIONS

In this case, FSTSMC performance is evaluated for the fixed initial conditions and different gain values. It shall be noted

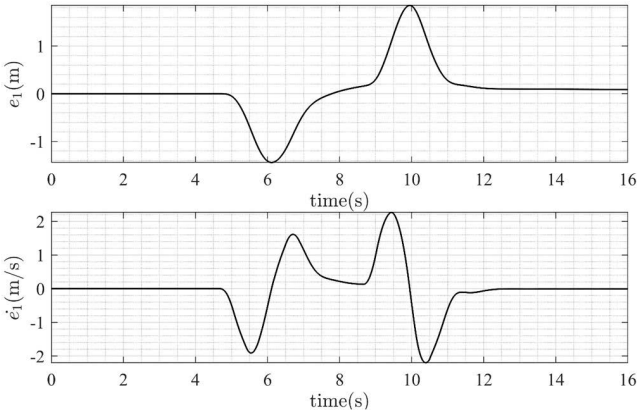

FIGURE 43. Lateral position and speed error at $v_x = 50\,km/h$.

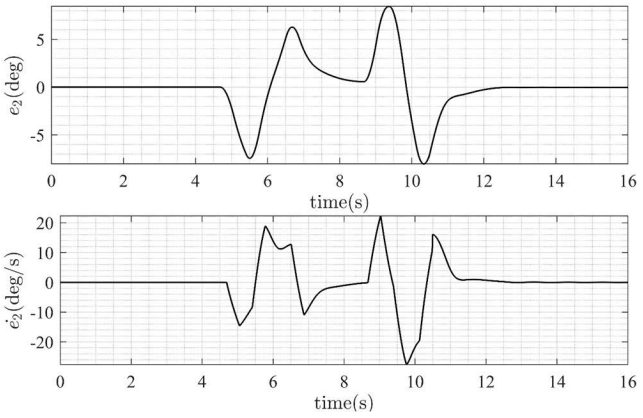

FIGURE 44. Yaw and Yaw rate error at $v_x = 50\,km/h$.

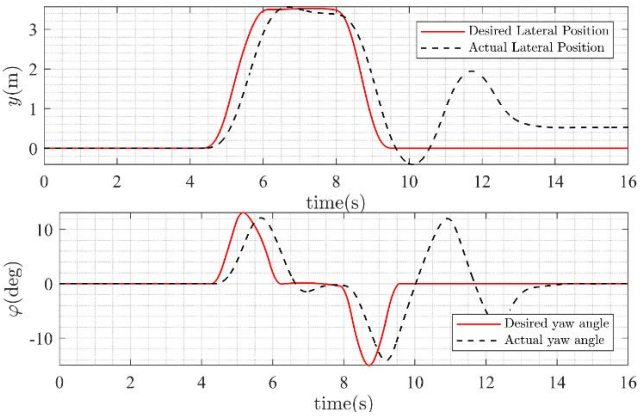

FIGURE 45. Tracking of lateral position and Yaw angle at $v_x = 55\,km/h$.

that the fixed time robust controller for two-time scale systems is not found in literature to the best of our knowledge. Therefore, it is not possible to provide its comparison with existing fixed time techniques.

The FSTSMC is implemented by setting the initial condition of $\varphi_0 = 0$. The limit of lateral position error $\hbar_1$ is set to $3m$ while that on yaw error is set to $\hbar_2 = 20°$. The allowable steady-state error margin $\rho = [\rho_1, \rho_2]$ is supposed

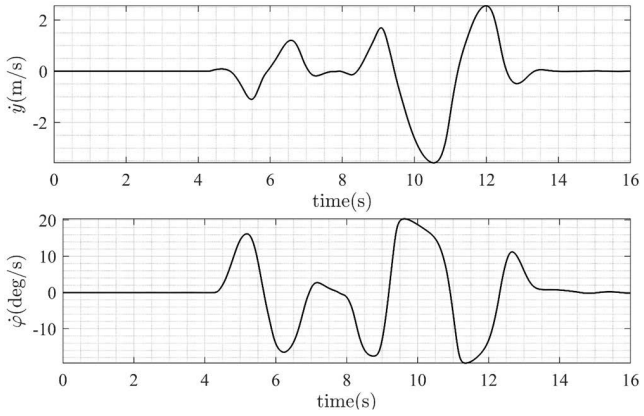

FIGURE 46. Lateral speed and Yaw rate at $v_x = 55km/h$.

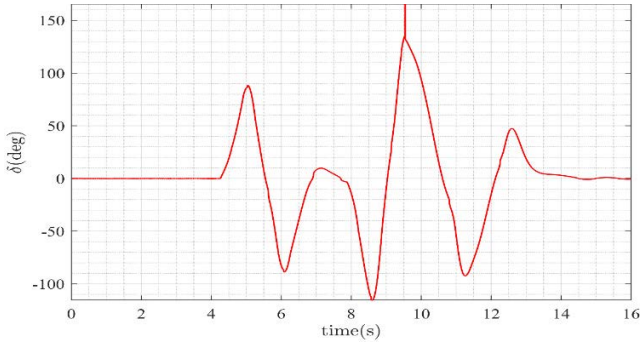

FIGURE 47. Steering angle at $v_x = 55km/h$.

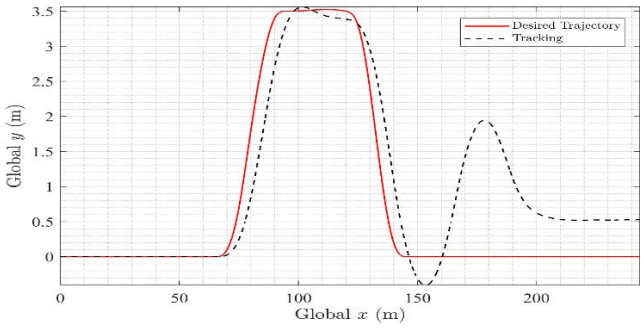

FIGURE 48. Trajectory tracking of self-driving car at $v_x = 50km/h$.

to be $[0.15m, 1°]$ while $a_1 = a_2$. The variations of the gains with the above control parameters result in different settling times. The simulation result for different gains and fixed initial condition is given in FIGURE 51.

From the figure, it is evident that for $\varphi_0 = 0$ and different gains results in different settling time to reach within the ρ bound. From the relation of fixed settling time (47), the fixed settling time of the system varies with the variations in the gains a_1 and a_2.

It can be seen from the FIGURE 51 if the gain is increased the output would require less time to reach and settle within ρ bound. The settling time values at different gains are given in Table 2. These values also satisfy (47).

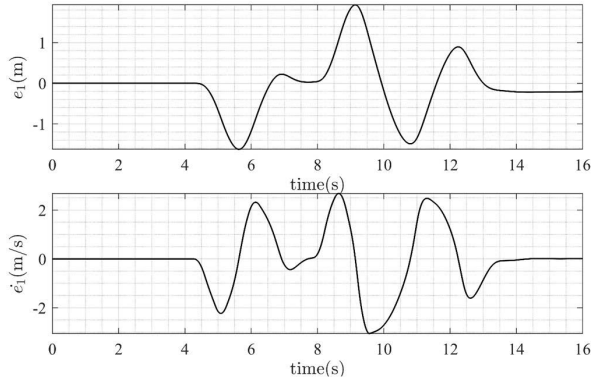

FIGURE 49. Lateral position and speed error at $v_x = 50km/h$.

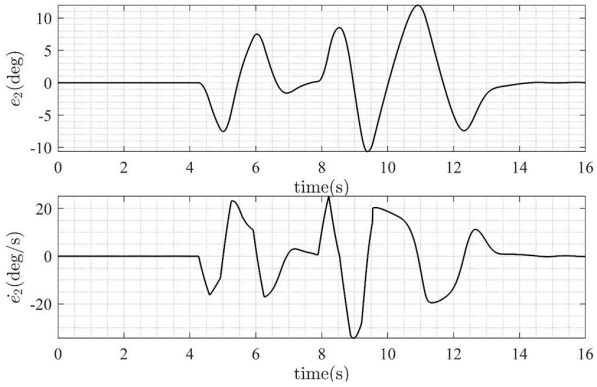

FIGURE 50. Yaw and Yaw rate error at $v_x = 55km/h$.

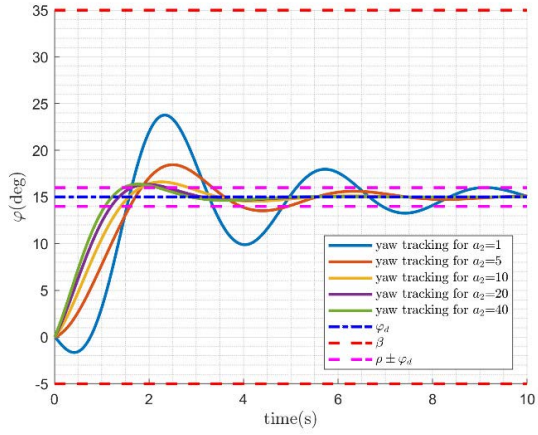

FIGURE 51. FSTSMC performance under varying gains and same initial condition.

D. FSTSMC PERFORMANCE FOR FIXED GAINS AND DIFFERENT INITIAL CONDITIONS

In this case, FSTSMC performance is evaluated for the fixed gain and different initial conditions. The FSTSMC is implemented by setting the gain of the controller to $a_1 = a_2 = 40$. The limit of lateral position error $\hbar_1$ is set to $3m$ while that on yaw error is set to $\hbar_2 = 20°$. The allowable steady-state error margin $\rho = [\rho_1, \rho_2]$ is supposed to be $[0.15m, 1°]$. The variation in initial conditions with the above control parameters results in the same settling time. The simulation

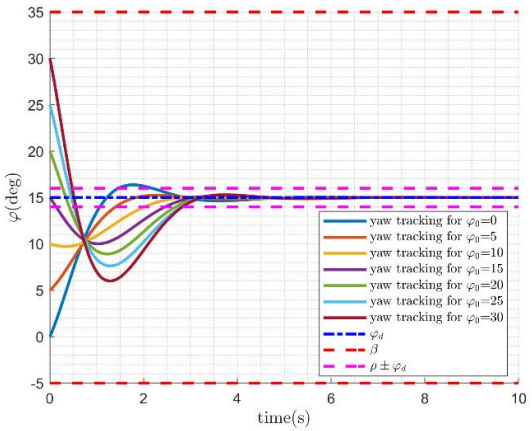

FIGURE 52. FSTSMC performance under fixed gain and different initial condition.

TABLE 2. FSTSMC performance under varying gains and same initial condition.

φ_0	Gain $a_1 = a_2 = a$	$T(sec)$
0	01	8.889
0	05	4.937
0	10	2.842
0	20	2.388
0	40	2.183

results for fixed gain and different initial conditions are given in FIGURE 52.

From the figure, it is evident that for $a_1 = a_2 = 40$ and different initial conditions, the settling time to reach within the ρ bound remains the same. From the relation of fixed settling time (47), the fixed settling time of the system is independent of initial conditions. It can be seen from the figure if the initial condition of the system varies there would not be any change in time to reach and settle within ρ bound. It is intuitive that higher the initial conditions (away from origin), the more control effort is required and vice versa.

E. DISCUSSION

The results depict that, generally, the performance of the proposed lateral controller tends to deteriorate with the increase in longitudinal speed or decrease in friction coefficient. The fluctuations in yaw at higher speeds and viscous surfaces cause a small steady-state error in the lateral position of self-driving cars. The lateral position error after the DLC maneuver is higher for low friction roads. The observations of simulations are summarized in Table 4. The following observations are made:

i) Higher steering input is required for higher longitudinal speeds.
ii) If longitudinal speed is kept constant, the magnitude of steering input needs to be higher for low friction road surfaces.

TABLE 3. FSTSMC performance for fixed gains and different initial conditions.

φ_0	Gain $a_1 = a_2 = a$	$T(sec)$
0	40	2.183
5	40	2.183
10	40	2.183
15	40	2.183
20	40	2.183
25	40	2.183
30	40	2.183

TABLE 4. Comparison of controller performance.

v_x	μ	δ_{max}	e_1^{MAX}	e_2^{MAX}	e_1^{SS}
40 km/h	0.85	77°	0.18m	6.3°	0
	0.5	85°	0.6m	6.4°	0
45 km/h	0.85	85°	0.19m	6°	0
	0.5	120°	0.72m	6°	0.07m
50 km/h	0.85	106°	0.2m	6.2°	0.03m
	0.5	96°	1.82m	8.5°	0.1m
55 km/h	0.85	114°	0.47m	5.25°	0.05m
	0.5	162°	1.9m	12°	0.49m

iii) After accomplishing the DLC maneuver, the steady-state lateral position error tends to increase for higher longitudinal speeds.
iv) After accomplishing the DLC maneuver, the steady-state lateral position is higher for a low friction road surface.
v) At higher longitudinal speeds, the performance of the two-time scale controller is not suitable.

VI. CONCLUSION

In this paper fixed settling time sliding mode control (FSTSMC) with barrier Lyapunov function is presented for a self-driving car. The path tracking control is developed to cater to the lateral dynamics of a self-driving car in the presence of unwanted disturbances and parametric uncertainties. Two-timescale based approach is employed to deal with the slow and fast dynamics of the vehicle separately. The fixed settling time sliding mode control (FSTSMC) with barrier Lyapunov function guarantees the convergence of tracking error within a certain pre-set bound in fixed time, for a two-timescale system. The path tracking ability of the proposed control scheme is validated using simulations based on CarSim and Simulink by ensuring the stable standard double-lane-change (DLC) maneuver of self-driving cars for different longitudinal speeds. It is observed that the proposed FSTSMC is a practical solution for the DLC problem of self-driving cars at slow longitudinal speeds. Moreover, the feature of guaranteeing the fixed settling time stability along with satisfying output constraints adds significance to the automotive industry. In future, the proposed control will be modified for time varying constraints and velocity constraints.

REFERENCES

[1] J. Levinson, J. Askeland, J. Becker, J. Dolson, D. Held, S. Kammel, J. Z. Kolter, D. Langer, O. Pink, V. Pratt, M. Sokolsky, G. Stanek, D. Stavens, A. Teichman, M. Werling, and S. Thrun, "Towards fully autonomous driving: Systems and algorithms," in *Proc. IEEE Intell. Vehicles Symp. (IV)*, Jun. 2011, pp. 163–168.
[2] Ü. Özgüner, T. Acarman, and K. A. Redmill, *Autonomous Ground Vehicles*. Norwood, MA, USA: Artech House, 2011.
[3] C. Badue, R. Guidolini, R. V. Carneiro, P. Azevedo, V. B. Cardoso, A. Forechi, L. Jesus, R. Berriel, T. M. Paixao, F. Mutz, and L. de Paula Veronese, "Self-driving cars: A survey," *Expert Syst. Appl.*, vol. 165, Mar. 2020, Art. no. 113816.
[4] M. H. Hebert, C. E. Thorpe, and A. Stentz, *Intelligent Unmanned Ground Vehicles: Autonomous Navigation Research at Carnegie Mellon*. New York, NY, USA: Springer, 2012.
[5] J. Li, H. Bao, X. Han, F. Pan, W. Pan, F. Zhang, and D. Wang, "Real-time self-driving car navigation and obstacle avoidance using mobile 3D laser scanner and GNSS," *Multimedia Tools Appl.*, vol. 76, no. 21, pp. 23017–23039, Nov. 2017.
[6] B. Paden, M. Čáp, S. Z. Yong, D. Yershov, and E. Frazzoli, "A survey of motion planning and control techniques for self-driving urban vehicles," *IEEE Trans. Intell. Vehicles*, vol. 1, no. 1, pp. 33–55, Jun. 2016.
[7] Q. Luo, Y. Cao, J. Liu, and A. Benslimane, "Localization and navigation in autonomous driving: Threats and countermeasures," *IEEE Wireless Commun.*, vol. 26, no. 4, pp. 38–45, Aug. 2019.
[8] R. Wang, H. Jing, C. Hu, F. Yan, and N. Chen, "Robust H_∞ path following control for autonomous ground vehicles with delay and data dropout," *IEEE Trans. Intell. Transp. Syst.*, vol. 17, no. 7, pp. 2042–2050, Feb. 2016.
[9] N. H. Amer, H. Zamzuri, K. Hudha, and Z. A. Kadir, "Modelling and control strategies in path tracking control for autonomous ground vehicles: A review of state of the art and challenges," *J. Intell. Robot. Syst.*, vol. 86, no. 2, pp. 225–254, May 2017.
[10] J. Guanetti, Y. Kim, and F. Borrelli, "Control of connected and automated vehicles: State of the art and future challenges," *Annu. Rev. Control*, vol. 45, pp. 18–40, May 2018.
[11] J. Huang, "Vehicle longitudinal control," in *Handbook of Intelligent Vehicles*. London, U.K.: Springer, 2012, pp. 167–190.
[12] B. Arifin, B. Y. Suprapto, S. A. D. Prasetyowati, and Z. Nawawi, "The lateral control of autonomous vehicles: A review," in *Proc. Int. Conf. Electr. Eng. Comput. Sci. (ICECOS)*, Oct. 2019, pp. 277–282.
[13] R. Rajamani, *Vehicle Dynamics and Control*. New York, NY, USA: Springer, 2011.
[14] C. M. Filho, D. F. Wolf, V. Grassi, and F. S. Osorio, "Longitudinal and lateral control for autonomous ground vehicles," in *Proc. IEEE Intell. Vehicles Symp.*, Jun. 2014, pp. 588–593.
[15] J. Zhao, H. Fu, D. Liu, G. Wang, and A. El Kamel, "Integrated longitudinal and lateral control system design and case study on an electric vehicle," *Math. Problems Eng.*, vol. 2019, pp. 1–13, Nov. 2019.
[16] D. Bevly, X. Cao, M. Gordon, G. Ozbilgin, D. Kari, B. Nelson, J. Woodruff, M. Barth, C. Murray, A. Kurt, and K. Redmill, "Lane change and merge maneuvers for connected and automated vehicles: A survey," *IEEE Trans. Intell. Vehicles*, vol. 1, no. 1, pp. 105–120, Mar. 2016.
[17] R. Marino, S. Scalzi, and M. Netto, "Nested PID steering control for lane keeping in autonomous vehicles," *Control Eng. Pract.*, vol. 19, no. 12, pp. 1459–1467, 2011.
[18] D.-C. Liaw and W.-C. Chung, "A feedback linearization design for the control of vehicle's lateral dynamics," *Nonlinear Dyn.*, vol. 52, no. 4, pp. 313–329, 2008.
[19] C. M. Kang, W. Kim, and C. C. Chung, "Observer-based backstepping control method using reduced lateral dynamics for autonomous lane-keeping system," *ISA Trans.*, vol. 83, pp. 214–226, Dec. 2018.
[20] P. Wang, S. Gao, L. Li, S. Cheng, and L. Zhao, "Automatic steering control strategy for unmanned vehicles based on robust backstepping sliding mode control theory," *IEEE Access*, vol. 7, pp. 64984–64992, 2019.
[21] W. Zhang, "A robust lateral tracking control strategy for autonomous driving vehicles," *Mech. Syst. Signal Process.*, vol. 150, Mar. 2021, Art. no. 107238.
[22] A. Norouzi, M. Masoumi, A. Barari, and S. Farrokhpour Sani, "Lateral control of an autonomous vehicle using integrated backstepping and sliding mode controller," *Proc. Inst. Mech. Eng., K, J. Multi-Body Dyn.*, vol. 233, no. 1, pp. 141–151, Mar. 2019.
[23] G. Tagne, R. Talj, and A. Charara, "Higher-order sliding mode control for lateral dynamics of autonomous vehicles, with experimental validation," in *Proc. IEEE Intell. Vehicles Symp. (IV)*, Jun. 2013, pp. 678–683.
[24] X. Wang, M. Fu, H. Ma, and Y. Yang, "Lateral control of autonomous vehicles based on fuzzy logic," *Control Eng. Pract.*, vol. 34, pp. 1–17, Jan. 2015.
[25] C. Hu, Y. Chen, and J. Wang, "Fuzzy observer-based transitional path-tracking control for autonomous vehicles," *IEEE Trans. Intell. Transp. Syst.*, vol. 22, no. 5, pp. 3078–3088, May 2021.
[26] W. Chen, R. Zhang, L. Zhao, H. Wang, and Z. Wei, "Control of chaos in vehicle lateral motion using the sliding mode variable structure control," *Proc. Inst. Mech. Eng., D, J. Automobile Eng.*, vol. 233, no. 4, pp. 776–789, Mar. 2019.
[27] K. Akermi, S. Chouraqui, and B. Boudaa, "Novel SMC control design for path following of autonomous vehicles with uncertainties and mismatched disturbances," *Int. J. Dyn. Control*, vol. 8, no. 1, pp. 254–268, Mar. 2020.
[28] C. Hatipoglu, U. Ozguner, and K. A. Redmill, "Automated lane change controller design," *IEEE Trans. Intell. Transp. Syst.*, vol. 4, no. 1, pp. 13–22, Mar. 2003.
[29] H. Zheng, Z. Huang, C. Wu, and R. R. Negenborn, "Model predictive control for intelligent vehicle lane change," in *Proc. ICTIS*, Jun. 2013, pp. 265–276.
[30] J. Nilsson and J. Sjoberg, "Strategic decision making for automated driving on two-lane, one way roads using model predictive control," in *Proc. IEEE Intell. Vehicles Symp. (IV)*, Jun. 2013, pp. 1253–1258.
[31] M. Mukai and T. Kawabe, "Model predictive control for lane change decision assist system using hybrid system representation," in *Proc. SICE-ICASE Int. Joint Conf.*, 2006, pp. 5120–5125.
[32] J. E. Naranjo, C. Gonzalez, R. Garcia, and T. D. Pedro, "Lane-change fuzzy control in autonomous vehicles for the overtaking maneuver," *IEEE Trans. Intell. Transp. Syst.*, vol. 9, no. 3, pp. 438–450, Sep. 2008.
[33] X. Huang, W. Lin, and B. Yang, "Global finite-time stabilization of a class of uncertain nonlinear systems," *Automatica*, vol. 41, no. 5, pp. 881–888, May 2005.
[34] A. Polyakov, "Nonlinear feedback design for fixed-time stabilization of linear control systems," *IEEE Trans. Autom. Control*, vol. 57, no. 8, pp. 2106–2110, Aug. 2012.
[35] A. Polyakov, D. Efimov, and W. Perruquetti, "Finite-time and fixed-time stabilization: Implicit Lyapunov function approach," *Automatica*, vol. 51, pp. 332–340, Jan. 2015.
[36] N. Mazhar, F. M. Malik, A. Raza, and R. Khan, "Predefined-time control of nonlinear systems: A sigmoid function based sliding manifold design approach," *Alexandria Eng. J.*, vol. 61, no. 9, pp. 6831–6841, Sep. 2022.
[37] H. Yu, K. Dai, H. Li, Y. Zou, X. Ma, S. Ma, and H. Zhang, "Distributed cooperative guidance law for multiple missiles with input delay and topology switching," *J. Franklin Inst.*, vol. 358, no. 17, pp. 9061–9085, Nov. 2021.
[38] L. Zhang, Y. Wang, Y. Hou, and H. Li, "Fixed-time sliding mode control for uncertain robot manipulators," *IEEE Access*, vol. 7, pp. 149750–149763, 2019.
[39] X. Jin, S.-L. Dai, and J. Liang, "Fixed-time path-following control of an autonomous vehicle with path-dependent performance and feasibility constraints," *IEEE Trans. Intell. Vehicles*, early access, Oct. 14, 2021, doi: 10.1109/TIV.2021.3119989.
[40] K. Xu, X. Wu, M. Ma, and Y. Zhang, "Energy-based output feedback control of the underactuated 2DTORA system with saturated inputs," *Trans. Inst. Meas. Control*, vol. 42, no. 14, pp. 2822–2829, Oct. 2020.
[41] H. T. Nguyen, M. T. Nguyen, T. T. Doan, and C. P. Vo, "Designing PID-fuzzy controller for pendubot system," *Robotica Manage.*, vol. 22, no. 2, pp. 21–27, 2017.
[42] D. Li, D. Zhao, Q. Zhang, and Y. Chen, "Reinforcement learning and deep learning based lateral control for autonomous driving [application notes]," *IEEE Comput. Intell. Mag.*, vol. 14, no. 2, pp. 83–98, May 2019.
[43] D. H. Vu, S. Huang, and T. D. Tran, "Hierarchical robust fuzzy sliding mode control for a class of simo under-actuated systems with mismatched uncertainties," *Telkomnika*, vol. 17, no. 6, pp. 3027–3043, 2019.
[44] D. Qian, J. Yi, and D. Zhao, "Hierarchical sliding mode control for a class of SIMO under-actuated systems," *Control Cybern.*, vol. 37, no. 1, p. 159, 2008.
[45] J. Jiang and A. Astolfi, "Lateral control of an autonomous vehicle," *IEEE Trans. Veh. Technol.*, vol. 3, no. 2, pp. 228–237, Jun. 2018.
[46] S. A. Ali Shah, B. Gao, N. Ahmed, C. Liu, and A. Rauf, "Disturbance observer-based sliding mode control of TORA system for floating wind turbines," in *Proc. IEEE 9th Annu. Int. Conf. CYBER Technol. Automat., Control, Intell. Syst. (CYBER)*, Jul. 2019, pp. 418–423, doi: 10.1109/CYBER46603.2019.9066505.

[47] J. Lee, R. Mukherjee, and H. K. Khalil, "Output feedback stabilization of inverted pendulum on a cart in the presence of uncertainties," *Automatica*, vol. 54, pp. 146–157, Apr. 2015.
[48] A. Chakrabortty and M. Arcak, "Time-scale separation redesigns for stabilization and performance recovery of uncertain nonlinear systems," *Automatica*, vol. 45, no. 1, pp. 34–44, Jan. 2009.
[49] A. Raza, F. M. Malik, N. Mazhar, H. Ullah, and R. Khan, "Finite-time trajectory tracking control of output-constrained uncertain quadrotor," *IEEE Access*, vol. 8, pp. 215603–215612, 2020.
[50] N. Ahmadian, A. Khosravi, and P. Sarhadi, "Managing driving disturbances in lateral vehicle dynamics via adaptive integrated chassis control," *Proc. Inst. Mech. Eng., K, J. Multi-Body Dyn.*, vol. 235, no. 1, pp. 122–133, Mar. 2021.
[51] K. P. Tee, S. S. Ge, and E. H. Tay, "Barrier Lyapunov functions for the control of output-constrained nonlinear systems," *Automatica*, vol. 45, no. 4, pp. 918–927, Apr. 2009.
[52] Y. Sun, D. Dong, H. Qin, and W. Wang, "Distributed tracking control for multiple Euler–Lagrange systems with communication delays and input saturation," *ISA Trans.*, vol. 96, pp. 245–254, Jan. 2020.
[53] C. Fu, W. Hong, H. Lu, L. Zhang, X. Guo, and Y. Tian, "Adaptive robust backstepping attitude control for a multi-rotor unmanned aerial vehicle with time-varying output constraints," *Aerosp. Sci. Technol.*, vol. 78, pp. 593–603, Jul. 2018.
[54] T. Jiang, D. Lin, and T. Song, "Finite-time backstepping control for quadrotors with disturbances and input constraints," *IEEE Access*, vol. 6, pp. 62037–62049, 2018.
[55] R. Potluri and A. K. Singh, "Path-tracking control of an autonomous 4WS4WD electric vehicle using its natural feedback loops," *IEEE Trans. Control Syst. Technol.*, vol. 23, no. 5, pp. 2053–2062, Sep. 2015.
[56] X. Jin, J. Wang, Z. Yan, L. Xu, G. Yin, and N. Chen, "Robust vibration control for active suspension system of in-wheel-motor-driven electric vehicle via μ-synthesis methodology," *J. Dyn. Syst., Meas., Control*, vol. 144, no. 5, May 2022, doi: 10.1115/1.4053661.
[57] W. Qin, "Unit sliding mode control for disturbed crowd dynamics system based on integral barrier Lyapunov function," *IEEE Access*, vol. 8, pp. 91257–91264, 2020.
[58] S. I. Han, J. Y. Cheong, and J. M. Lee, "Barrier Lyapunov function-based sliding mode control for guaranteed tracking performance of robot manipulator," *Math. Problems Eng.*, vol. 2013, Oct. 2013, Art. no. 978241.
[59] R. Khan, F. M. Malik, N. Mazhar, A. Raza, R. A. Azim, and H. Ullah, "Robust control framework for lateral dynamics of autonomous vehicle using barrier Lyapunov function," *IEEE Access*, vol. 9, pp. 50513–50522, 2021.
[60] B. Zhu, X. Wang, and K.-Y. Cai, "Approximate trajectory tracking of input-disturbed PVTOL aircraft with delayed attitude measurements," *Int. J. Robust Nonlinear Control*, vol. 20, no. 14, pp. 1610–1621, Sep. 2010.
[61] M. Innocenti, L. Greco, and L. Pollini, "Sliding mode control for two-time scale systems: Stability issues," *Automatica*, vol. 39, no. 2, pp. 273–280, 2003.
[62] H. K. Khalil, *High-Gain Observers in Nonlinear Feedback Control*. Philadelphia, PA, USA: SIAM, 2017.
[63] B. Ren, S. S. Ge, K. P. Tee, and T. H. Lee, "Adaptive neural control for output feedback nonlinear systems using a barrier Lyapunov function," *IEEE Trans. Neural Netw.*, vol. 21, no. 8, pp. 1339–1345, Aug. 2010.
[64] Y. Sun, B. Chen, C. Lin, and H. Wang, "Finite-time adaptive control for a class of nonlinear systems with nonstrict feedback structure," *IEEE Trans. Cybern.*, vol. 48, no. 10, pp. 2774–2782, Oct. 2017.
[65] A. Raza, F. M. Malik, N. Mazhar, and R. Khan, "Two-time-scale robust output feedback control for aircraft longitudinal dynamics via sliding mode control and high-gain observer," *Alexandria Eng. J.*, vol. 61, no. 6, pp. 4573–4583, Jun. 2022.

RAMEEZ KHAN received the B.S. degree in electronics engineering from COMSATS, Abbottabad, Pakistan, in 2012, and the M.S. degree in electrical engineering from the National University of Science and Technology, Islamabad, Pakistan, 2014, where he is currently pursuing the Ph.D. degree. His research interests include the development of nonlinear observers and robotic control systems.

RAJA AMER AZIM received the B.E. degree in mechanical engineering from the University of Engineering and Technology, Taxila, Pakistan, in 1993, the M.S. degree in mechanical engineering from the University of New South Wales, Australia, in 2001, and the Ph.D. degree in mechanical engineering, in 2015. He joined the Faculty of Department of Mechanical Engineering, College of EME, National University of Sciences and Technology, Islamabad, Pakistan, where he is currently working as an Assistant Professor with the Department of Mechanical Engineering, College of EME, with over two decades of experience in mechanical product development in research and development and academic organizations. He has various reputed journal and conference publications to his name. He is working on several funded research projects. His research interests include vehicle dynamics and control systems, mechanical system design, and autonomous vehicle systems.

FAHAD MUMTAZ MALIK received the B.Sc., M.S., and Ph.D. degrees from the National University of Sciences and Technology, Islamabad, Pakistan, in 2004, 2006, and 2009, respectively. He is currently a Professor and the Head of Department with the Department of Electrical Engineering, College of Electrical and Mechanical Engineering, National University of Sciences and Technology. He is the author of over 80 papers in peer-reviewed international journals and conferences. His research interests include the control of service and field robots, reinforcement learning, artificial intelligence, and nonlinear control systems.

NAVEED MAZHAR received the B.S. degree in electronics engineering from COMSATS, Abbottabad, Pakistan, in 2013, and the M.S. degree in electrical engineering from the National University of Science and Technology, Islamabad, Pakistan, in 2016, where he is currently pursuing the Ph.D. degree. His research interests include multi-agent systems, modeling, networked control systems, fixed-time control, and linear and nonlinear control design.

ABID RAZA received the B.S. degree in electronics engineering from COMSATS, Abbottabad, Pakistan, in 2012, and the M.S. degree in electrical engineering from the National University of Science and Technology, Islamabad, Pakistan, in 2014, where he is currently pursuing the Ph.D. degree. His research interests include nonlinear control, high gain observers, multi-time scale systems, flight control systems, robust control of UAVs, and robotics.

HAMEED ULLAH received the B.Sc. degree in electrical engineering from UET, Peshawar, Pakistan, in 2015, and the M.S. degree in electrical engineering from the National University of Sciences and Technology (NUST), Islamabad, Pakistan, in 2019. He is currently pursuing the Ph.D. degree with the PRISMA Laboratory, Department of Electrical Engineering and Information Technology (DIETI), University of Naples Federico II—UNINA, Italy. His research interests include UAVs, aerial robotics, robotic manipulators, robust state estimation, linear and nonlinear control systems, modeling, and robust nonlinear control for underactuated mechanical systems.